Petroleum Science 23 (2026) 2404–2434

Contents lists available at ScienceDirect

Petroleum Science

journal homepage: www.keaipublishing.com/en/journals/petroleum-science

Original Paper

A new approach for analyzing the formation and evolution of the Mesoproterozoic petroleum system in the Ordos Basin, China: Insights from a nested simulation with local grid refinement

Kuai-Le Zhang [a,b], Zhen-Liang Wang [a,b,*], Xiao-Rong Luo [a,b], Xing Pan [c,d], Li-Yong Fan [c,d], Zhan-Rong Ma [c,d]

[a] State Key Laboratory of Continental Dynamics and Department of Geology, Northwest University, Xi'an, 710069, Shaanxi, China
[b] Department of Geology, Northwest University, Xi'an, 710069, Shaanxi, China
[c] Exploration and Development Research Institute of PetroChina Changqing Oilfield Company, Xi'an, 710018, Shaanxi, China
[d] National Engineering Laboratory for Exploration and Development of Low-Permeability Oil & Gas Fields, Xi'an, 710018, Shaanxi, China

ARTICLE INFO

Article history:
Received 25 November 2024
Received in revised form
24 November 2025
Accepted 3 March 2026
Available online 7 March 2026

Edited by Xiu-Fang Hu

Keywords:
Ordos Basin
Mesoproterozoic
Petroleum system
Basin simulation
Hydrocarbon accumulation

ABSTRACT

The study on Meso–Neoproterozoic petroleum systems has attracted extensive attention. However, it still faces some problems such as the availability of hydrocarbon accumulating elements, complexity of accumulation process, and limited petroleum geology data. This study focuses on the Mesoproterozoic petroleum system in the Ordos Basin. By analyzing hydrocarbon accumulation factors, the hydrocarbon migration simulation at the migration and accumulation system scale is integrated into the source rocks evolution simulation at the petroleum system scale. The evolution of the Mesoproterozoic petroleum system was reconstructed using profile and plan views of multi-critical periods. The hydrocarbon migration process of each hydrocarbon accumulation unit was analyzed by hydrocarbon accumulation dynamics, and the simulation results of the hydrocarbon accumulation during each period were superimposed in a single stratum according to its sequence and spatial position to examine the type of each hydrocarbon accumulation and the regularities of the oil–gas distribution. Finally, a methodology comprising five figures and one table was developed to characterize the Mesoproterozoic petroleum system and assess prospective areas. The results of this study are as follows. (1) The plan view and profile of multi-critical periods indicate that the distribution of the Central Paleohigh controlled the hydrocarbon migration and accumulation in the Triassic–Early Cretaceous, during which the oil–gas reservoirs were primarily distributed within the paleohigh and its adjacent region, and oil and gas readjustment and re-accumulation have occurred along the unconformity towards the northeastern region on a large scale since the Late Cretaceous. (2) Integration of the regional geologic setting and some petroleum geology data suggests that in the Changcheng System, the structural highs and unconformity-related traps are of crucial importance for current oil exploration, and the Cambrian weathering crust in the southwestern part of the basin contains abundant oil–gas shows, highlighting the contribution of the Mesoproterozoic petroleum system.
© 2026 The Authors. Publishing services by Elsevier B.V. on behalf of KeAi Communications Co. Ltd. This is an open access article under the CC BY-NC-ND license (http://creativecommons.org/licenses/by-nc-nd/4.0/).

1. Introduction

The Mesoproterozoic to Neoproterozoic represented a stage of substantial change in the evolution of Earth (Santos et al., 2000; Butterfield, 2015; Wang et al., 2023). During this period, atmospheric oxygen content increased, and biodiversity boosted. This led to sufficient material foundation for the development of source rocks (Javaux et al., 2001; Craig et al., 2013). The discovery of several oil and gas reservoirs, seepages, and organic-rich rocks

* Corresponding author.
E-mail address: wangzl@nwu.edu.cn (Z.-L. Wang).
Peer review under the responsibility of China University of Petroleum (Beijing).

https://doi.org/10.1016/j.petsci.2026.03.007
1995-8226/© 2026 The Authors. Publishing services by Elsevier B.V. on behalf of KeAi Communications Co. Ltd. This is an open access article under the CC BY-NC-ND license (http://creativecommons.org/licenses/by-nc-nd/4.0/).

within the Proterozoic strata worldwide highlighted the substantial potential of Meso–Neoproterozoic petroleum systems (Craig et al., 2009; Frolov et al., 2015; Qu et al., 2020; Faiz et al., 2022). In China, the organic-rich source rocks, and the existence of primary oil–gas reservoirs have also been identified within the Meso–Neoproterozoic strata in the North China Craton (NCC) (Liu et al., 2011; Li et al., 2014; Luo et al., 2016; Wang et al., 2017, 2018, 2019, 2022; Jiang et al., 2023; Wu et al., 2024a). Moreover, the search for oil–gas reservoirs in deeper and more ancient strata is becoming an increasingly significant focus in global hydrocarbon exploration (Jin, 2023; Zhu et al., 2024). This trend underscores the critical importance of studying Meso–Neoproterozoic petroleum systems.

The theory of petroleum systems, serving as one of the cornerstone theories in modern petroleum geology, offers a critical scientific foundation for the exploration and development of oil–gas resources. Since Dow (1974) introduced the concept of "Oil System", and Magoon and Dow (1994) further developed the theory of "Petroleum System" by presenting core research contents in the form of "four figures and one table", that is, burial history map, plan view of the critical period, profile of the critical period, accumulation events chart, and reserves and type description table, which have been widely recognized. To guide oil and gas exploration further effectively, Magoon and Schmoker (2000) introduced the concept of "Total Petroleum System", which includes all known accumulations related to the mature source rock pod(s) as well as complementary areas with petroleum potential linked to these pods. When combined with the assessment unit method, this approach proves to be more appropriate for resource assessment (Pollastro et al., 2007). With the discovery and exploration of unconventional oil–gas, Jia et al. (2023) proposed the concept of "Whole Petroleum System", which incorporates the research content of unconventional oil–gas, aiming to facilitate the integrated exploration and development of both conventional and unconventional oil–gas resources. However, due to the limited availability of oil–gas geological data, the comprehensive investigation of the Meso–Neoproterozoic whole petroleum systems may present significant challenges. Additionally, traditional Meso–Neoproterozoic petroleum systems also face numerous unresolved issues.

Owing to the protracted geological evolution and intense multistage tectonic movement (Du et al., 2019), the Meso–Neoproterozoic petroleum systems are highly complex, and their research face the following problems. First, the distribution and availability of hydrocarbon accumulating elements require further clarification. The intense multistage tectonic movement has led to intricate patterns in the distribution of elements such as source rocks, reservoir rocks and seal rocks, which form a critical basis for studying the Meso–Neoproterozoic petroleum systems. Second, there are diverse hydrocarbon sources. During the burial of the Mesoproterozoic strata, they entered the oil-generation and gas-generation windows, and the sequence and retention time of the source rocks in different regions varied. Consequently, the processes of hydrocarbon generation and expulsion often occurred in multiple stages. Furthermore, due to the significant burial depth of the Mesoproterozoic strata, early crude oil cracking may have led to the development of new gas sources, contributing to the diversity of the oil and gas sources (Luo et al., 2016; Faiz et al., 2022). Third, multistage hydrocarbon migration and accumulation occurred. During the prolonged geological period, there was a complex interplay between the multistage hydrocarbon generation and expulsion. Furthermore, the occurrence of multistage tectonic movement and uplift-erosion within the Meso–Neoproterozoic petroleum systems led to destruction and readjustment of the hydrocarbon reservoirs accumulated in the earlier stage. These processes ultimately resulting in multistage hydrocarbon migration, accumulation, and loss within the petroleum system (Zhao et al., 2001a, 2001b). Fourth, there are limited petroleum geology data and incomplete evidence on accumulation. While the Meso–Neoproterozoic source rocks are widely distributed, the related oil–gas plays remain relatively limited and localized (Faiz et al., 2022; Jiang et al., 2023; Wu et al., 2024a). Furthermore, the thermal evolution degree of the Meso–Neoproterozoic strata in China is generally at a high level, with a scarcity of live oil, resulting in incomplete evidence for hydrocarbon accumulation (Wang and Han, 2011).

The Meso–Neoproterozoic petroleum systems involve multiple critical episodes of hydrocarbon generation, migration, and accumulation. Traditional "four figures and one table" method, which was originally developed for single-period oil–gas accumulation, is inadequate for characterizing such complexity. It primarily emphasizes accumulating elements and their coupling processes during only one episode of migration and accumulation, thus failing to adequately address the petroleum system evolution characterized by multiple critical episodes. In addition, analyzing the formation and evolution of the Meso–Neoproterozoic petroleum systems presents a significant challenge. The petroleum migration and accumulation unit, which encompasses source rocks or destroyed reservoirs, pathway system, traps, and the dynamic processes of migration from sources to traps (Luo, 2008), provides a concise description of the accumulation process within a single petroleum system. Based on this, Luo et al. (2020) proposed a method for simulating hydrocarbon migration in superimposed basins by splitting multiple periods of hydrocarbon generation, migration, and accumulation processes, which correspond to distinct stages of basin subsidence and inversion. However, precise control of the injection positions (layer or fault) and fluxes along the outer boundary of the target area is critical for ensuring the accuracy of simulation results. In conclusion, considering the challenges such as the availability of hydrocarbon-accumulating elements, the complexity of accumulation processes, and the limited petroleum geology data in Meso–Neoproterozoic petroleum systems, it is essential to systematically integrate source rocks evolution at the petroleum system scale with hydrocarbon accumulation dynamics at the migration and accumulation unit scale, in order to analyze the formation and evolution of petroleum systems.

The Ordos Basin, located in the southern margin of the NCC, contains three sets of petroleum systems in the Mesozoic, Paleozoic, and Mesoproterozoic strata. The first two petroleum systems have been confirmed to possess abundant oil and gas resources (Fu et al., 2013; Yang and Liu, 2014). Recent studies on the tectonic evolution and lithofacies paleogeography during the Mesoproterozoic, as well as types and characteristics of the source rocks in the Cuizhuang Formation, have confirmed the presence of potential source rocks (Li et al., 2019; Pan et al., 2020; Bai et al., 2022; Wu et al., 2024a). Furthermore, numerous bitumen shows have been discovered in the areas surrounding the Ordos Basin (Li et al., 2011; Pan et al., 2020), as well as in typical well locations (Wells GT1 and T59) within the basin. Despite the limited amount of research conducted on the source and reservoir rocks in the deep Mesoproterozoic strata and the relatively low exploration level, insights derived from the current exploration and research indicate that there is still some potential for gas accumulation in the Mesoproterozoic strata (Hao et al., 2016; Du et al., 2019; Fu et al., 2019).

In this study, we focused on the Mesoproterozoic petroleum system in the Ordos Basin. Based on an analysis of hydrocarbon accumulation factors, we integrated hydrocarbon migration simulation at the migration and accumulation system scale with source rocks evolution simulation at the petroleum system scale.

The hydrocarbon migration process of each accumulation unit was then analyzed using a hydrocarbon accumulation dynamics approach. To characterize the Mesoproterozoic petroleum system, we developed an approach consisting of five figures and one table: burial history map, accumulation events chart, plan view of multi-critical periods, profile of multi-critical periods, superimposed multi-period accumulation map for a single stratum, and a table summaring the reserves and types of discoveries or simulations. This study provides a novel approach for analyzing the Meso–Neoproterozoic petroleum systems and essential insights for future hydrocarbon exploration in the Ordos Basin.

2. Methodology

2.1. Nested simulation with local grid refinement

Meso–Neoproterozoic petroleum systems have emerged as a new focal point for petroleum exploration on a global scale. However, the petroleum geology data available for these systems are relatively limited and unevenly distributed, resulting in qualitative speculation in many regions. This poses challenges in accurate geological modeling at the basin or petroleum system scale. However, conducting only evolution simulation of the source rocks can still yield reliable results with relatively coarse geological modeling. This is because regardless of whether the grid resolution is 10 km × 10 km or 1 km × 1 km, it has little impact on the hydrodynamic pattern and thermal maturity of the source rocks.

The hydrocarbon migration and accumulation unit is a three-dimensional (3-D) geologic unit positioned between the petroleum system and the hydrocarbon accumulation play (Fig. 1(a)), enabling the entire process of hydrocarbon migration and accumulation to be realized (Zhao et al., 2001a, 2001b). The migration and accumulation units with favorable accumulation conditions are often the target area for exploration. It is crucial to gather as much comprehensive data as possible in order to analyze the potential oil–gas distribution. The nested simulation involves nesting the refinement model of the target region, which has abundant data, within a coarse petroleum system model (Hantschel and Kauerauf, 2009). This allows for the connection of the widely distributed source rocks with the target area. The nested simulation with local grid refinement, without significantly increasing the total number of grid cells, enhances the resolution of the target area and reduces the demand for computing resources (Xu and Sepehrnoori, 2022; Zhang et al., 2023).

The essence of nested simulation for local grid refinement lies in analyzing hydrocarbon migration and accumulation processes within the refined model of the target area, while also taking into account the influence of potential hydrocarbon sources external to the target region. Consequently, basin modeling at varying scales will exhibit distinct characteristics. For evolution modeling of source rocks at the basin scale, input parameters such as the thickness of the source rock, type of organic matter, kinetics of the hydrocarbon generation, and heat flow should be characterized. Additionally, below the regional caprocks, analysis of the merging and splitting of the migration and accumulation units in the evolution history should be conducted to effectively divide the migration and accumulation unit (system). At the unit scale, it was necessary to further characterize the input parameters related to hydrocarbon migration, such as the reservoir–caprock assemblage, pathway system, and fluid dynamics.

During the nesting process, it is crucial to dynamically adjust both the parent and child models in accordance with the fluid conditions at their interfaces to ensure consistency in the simulation results. Specifically, ensuring the injection modes, layers, and the fluxes of hydrocarbons generated outside the child model constitutes a critical aspect of nested simulation. This can be achieved by adding additional grids and introducing the additional coupling conditions. Generally, the sedimentary facies of the parent and child models are consistent. However, due to differences in grid resolution, the meshing results for certain facies exhibit notable inconsistencies. As shown in Fig. 1(c), the grid cells C_1 and C_2 in the parent model, which contain a lower proportion of conduit system facies, are discretized as non-conduit system facies, leading to hydrocarbon injection through the boundary cells (Q_1, Q_2) may not result in effective migration or accumulation within regions A and B. By adding additional grids into the parent model near the interfaces between the parent and child models, the discretization of polygonal boundary faces associated with hydrocarbon injection is refined, thereby improving the accuracy of hydrocarbon injection into the target zones and potentially leading to significantly different outcomes (Fig. 1(d)). However, the polygonal boundary surfaces associated with hydrocarbon injection in the two models remain incompletely aligned. To address this issue, coupling conditions can be established according to the requirement of local conservation, as follows:

$$Q = \sum_{i=1}^{n} k_i \times Q_i$$

where Q is the known polygon boundary face fluxes in the parent model, and k_i and Q_i are the permeability and flux of the i-th polygon boundary face in the child model corresponding to the parent model, respectively.

By adding additional grids and introducing the additional coupling conditions, the hydrocarbons generated by the parent model can be accurately injected into the child model, thereby enabling the nesting of hydrocarbon migration simulation at the scale of the hydrocarbon migration and accumulation unit (system) within the evolution simulation of the source rocks at the scale of the petroleum system (Fig. 1(b)). This integrated approach aims to enhance the accuracy of simulation results.

2.2. Accumulation process in complex petroleum systems

In one simple petroleum system, if there has been only one period of migration and accumulation event with well-documented timing, the accumulation process can be described succinctly as source rocks–pathways–traps model. However, analyzing the Mesoproterozoic petroleum system with complexity of multi-kitchen and multi-stage hydrocarbon generation, migration, and accumulation, as well as multi-stage readjustment and re-accumulation, presents a significant challenge. The concept of migration and accumulation units, which can be temporally and spatially defined according to the stages of migration and accumulation, enables the subdivision of a complex system into several simpler units (Luo et al., 2020). This allows for individual units to be analyzed in terms of their respective timing of hydrocarbon charging. Finally, the dynamic processes of hydrocarbon accumulation could be reconstructed, unit by unit and period by period. As shown in Fig. 1(e), during the first critical period, the source rocks linked to Unit 2 commenced hydrocarbon generation, and the sealing of Fault 1 resulted in the formation of oil reservoir. During the second critical period, the source rocks related to both Unit 1 and Unit 2 began to mature on a large scale, and oil reservoirs accumulated in the structural highs of both units due to cross-fault leaking along Fault 1. During the third critical period, Fault 2 reopened vertically, establishing a connection between the two units. At this time, the source rocks entered the gas-generating stage and early crude oil began to undergo thermal cracking,

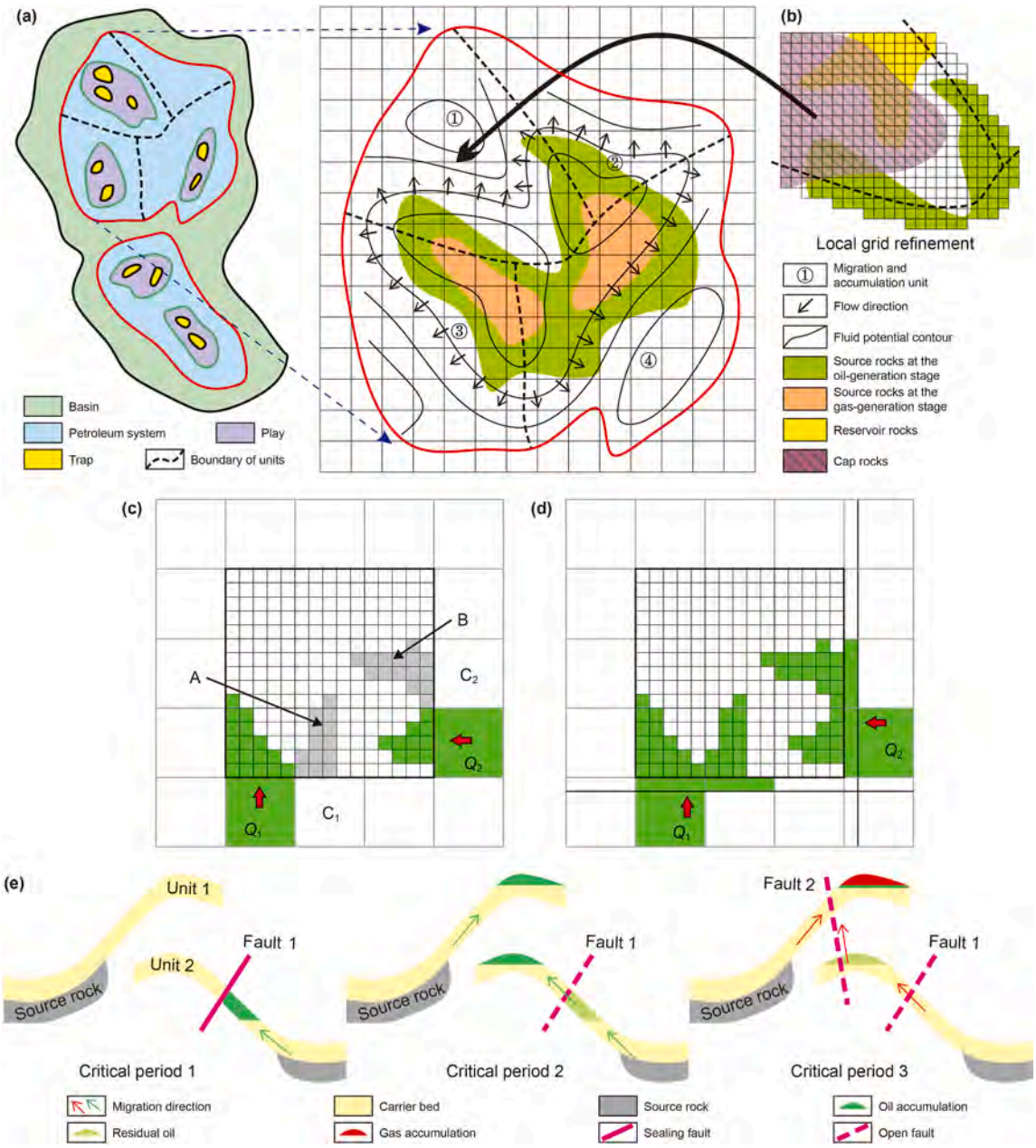

Fig. 1. **(a)** Sketch map showing the research scale of the hydrocarbon accumulation, **(b)** nested migration and accumulation unit grid refinement to improve the simulation resolution, **(c)** simple nested simulation and its potential simulation results, **(d)** potential simulation results after adding additional grids into the parent model, and **(e)** the analysis of the hydrocarbon accumulation process unit by unit and period by period.

which ultimately led to the formation of a gas reservoir at the structural high of Unit 1.

Based on the nested simulation results and above concepts, through delineation of the main accumulation periods and division of the migration and accumulation units, the dynamic processes of hydrocarbon migration, accumulation and readjustment for each hydrocarbon accumulation pool were reconstructed. This analysis was carried out unit by unit and period by period, based on the pathway system, cap rock, reservoir rock, and trap distribution, to determine the type and characteristics of each hydrocarbon accumulation pool in each period, such as oil–gas reservoirs that have undergone multi-stage accumulation from the source kitchen to the trap, those that have experienced failure and leakage of earlier formed accumulation pools, and those that have readjusted from ancient reservoirs to new ones. Notably, the hydrocarbon sources during this process encompassed various factors, including hydrocarbon expulsion from source rocks, oil overflow from ancient reservoirs, and gas generation via thermal cracking in ancient oil reservoirs.

2.3. Core figures and tables for Meso–Neoproterozoic petroleum systems

Traditional method of four figures and one table for single period oil–gas accumulation is inadequate for characterizing complex Meso–Neoproterozoic petroleum systems. For the Meso–Neoproterozoic petroleum systems with limited petroleum geology data and complex accumulation processes, the hydrocarbon migration simulation at the scale of migration and accumulation system was nested into the source rock evolution modeling

at the petroleum system scale, and the migration dynamics of each accumulation unit was analyzed using a hydrocarbon accumulation dynamics approach. Then, the nested simulation results of the hydrocarbon accumulation during each period were superimposed in a single stratum according to its sequence and spatial position, and a five-figures-and-one-table approach was developed (Fig. 2), including a burial history map, an accumulation events chart, a plan view of multi-critical periods, a profile of multi-critical periods, a superimposed map of hydrocarbon accumulation in different periods of a single stratum, and a reserves and type description table for discoveries or simulations, to characterize complex Meso–Neoproterozoic petroleum systems and identify favorable exploration areas.

2.4. Trace and rare earth element analysis

The trace and rare earth element (REE) analysis was conducted using an Agilent 7500a plasma mass spectrometer (USA) at the State Key Laboratory of Continental Dynamics, Northwest University (Xi'an). Fifty milligrams of sample were weighed into a Teflon microwave digestion vessel, dissolved in a mixture of 1.5 mL 65% nitric acid (HNO_3), 1.5 mL 40% hydrofluoric acid (HF), and 0.01 mL 70% perchloric acid ($HClO_4$), and then evaporated to near dryness on a hot plate at 140 °C. Then, it was redissolved in a mixture of 1.5 mL HNO_3 and 1.5 mL HF, sealed, and heated in an oven at 190 °C for 48 h, followed by evaporation to near dryness on a hot plate after cooling. Subsequently, 3.0 mL of 50% HNO_3 was added, the vessel was sealed, and the mixture was heated in an oven at 150 °C for 12 h, after which the resulting solution was transferred to a PET beaker. Finally, an internal standard solution containing rhodium (Rh) and deionized water were added to the sample for measurement, ensuring that the final Rh concentration in the solution was 10 ng/mL. Precision and accuracy were assessed through repeated analyses of the sample and four internationally recognized reference materials (AGV-2, BCR-2, BHVO-2, and GSP-2). The analytical precision was higher than ±5%.

3. Geologic setting and hydrocarbon accumulation factors

3.1. Tectonic evolution, stratigraphy, and sedimentation

The NCC is one of the oldest cratons in the world and records nearly all of the major geological events that occurred in the early geotectonic history (Diwu et al., 2008; Zhai, 2010). In the context of the Columbia supercontinent's breakup, the NCC experienced an extensional tectonic setting during the Mesoproterozoic (Zhao et al., 2003; Lu et al., 2008; Peng et al., 2011; Zhang et al., 2012, 2013; Li et al., 2024). Following a series of volcanic activity during the Early Mesoproterozoic (1.78–1.75 Ga) (Zhao et al., 2009),

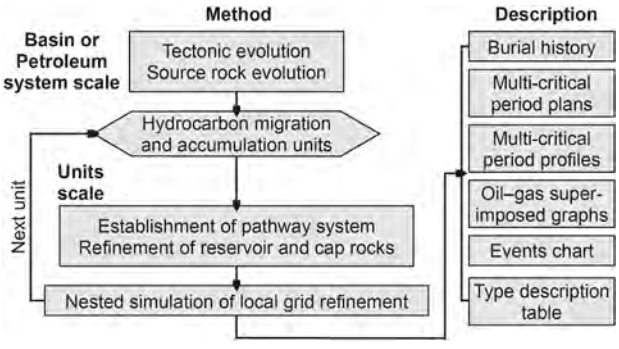

Fig. 2. Flowchart showing the steps for analyzing the Mesoproterozoic petroleum system.

sedimentary layers predominantly formed within three primary rifts: the Xiong'er Rift in the southern part of the NCC, the Yan–Liao Rift in the central part of the NCC, and the Baiyun Obo–Zhaertai–Langshan (BZL) Rift in the northern part of the NCC (Fig. 3(b)) (Zhao et al., 2002; Cui et al., 2011; Zhai et al., 2014; Li et al., 2019).

In this tectonic setting, a series of rifts also developed in the Ordos Basin, with the largest ones forming along its southern and western margins. The southern rift was the westward extension of the Xiong'er Rift system, while the western Helan Rift resulted from the reactivation of the junction belt between the Alxa and Ordos ancient continental blocks (Chen, 2015). Building on the large-scale rifts along the southern and western margins, branching rifts developed in a northeast direction, extending into the interior of the Ordos Block. These included the Ning–Meng (N–M) Rift, the Dingbian (DB) Rift, and the Jin–Shan (J–S) Rift. The thickness, length, and width of the Changcheng System in each rift were mainly within the ranges of 2000–3000 m, 250–300 km, and 50–100 km, respectively. The thickness of the Changcheng System on the reliefs between the rifts was significantly smaller, typically less than 1000 m, resulting in a sedimentary pattern characterized by alternating uplifts and depressions (Fig. 3(c)). After the Mesoproterozoic rift stage, the Ordos Basin underwent a series of geological developments, including a passive margin basin during the Cambrian–Middle Ordovician, a collisional orogeny in the Late Ordovician, peripheral rifting in the Late Carboniferous–Permian, a depression basin in the Early Mesozoic, a peripheral foreland basin in the Middle–Late Mesozoic, and finally a peripheral faulted depression in the Cenozoic (Wang et al., 2021; Yang et al., 2021a; Gao et al., 2022; Xu and He, 2022).

The strata in the Ordos Basin are relatively well-developed, featuring Meso–Neoproterozoic to Early Paleozoic neritic clastic rocks and carbonate platform deposits, as well as Late Paleozoic–Cenozoic continental clastic rock deposits, with an average total thickness of about 6000 m (Fig. 3(d)). The filling process in the Zhongtiao Mountains during the Meso–Neoproterozoic can be divided into two stages. First, during the rift depression period, as transgression progressed, littoral and neritic shelf sedimentary series were formed, including the interbedded sandstones and thin shales of the Baicaoping Formation, the quartz sandstones of the Beidajian Formation, and the thick shales and sandstones of the Cuizhuang Formation, which was the main stratum for the distribution of potential source rocks. Second, during the epicontinental sea sedimentary period, the Luoyukou and Longjiayuan formations, characterized by carbonate platform facies, were deposited (Wang et al., 2018; Pan et al., 2020). The Qingbaikou–Nanhua System is largely absent in the basin, and the Sinian System is only present in scattered areas in the western and southern margins of the basin. Additionally, the Silurian, Devonian, and Lower Carboniferous series are entirely absent overall. During the Cambrian Mantou–Xuzhuang period, the extent of transgression in the basin significantly expanded, resulting in the deposition of marine shale and tight carbonatite within the transgressive systems tract. These deposits, together with the Ordovician marine shale and evaporite, are the regional caprocks of the Mesoproterozoic petroleum system (Fig. 4).

3.2. Source rocks

3.2.1. Characteristics and distribution

Black shale and carbonaceous shale are widely distributed in outcrops surrounding the Ordos Basin, as well as in typical wells in the Mesoproterozoic System within the basin. It has been discovered that there are good Mesoproterozoic source rocks in the Yinshan area on the northern margin and in the Qinling orogenic belt on the southern margin, indicating a significant hydrocarbon

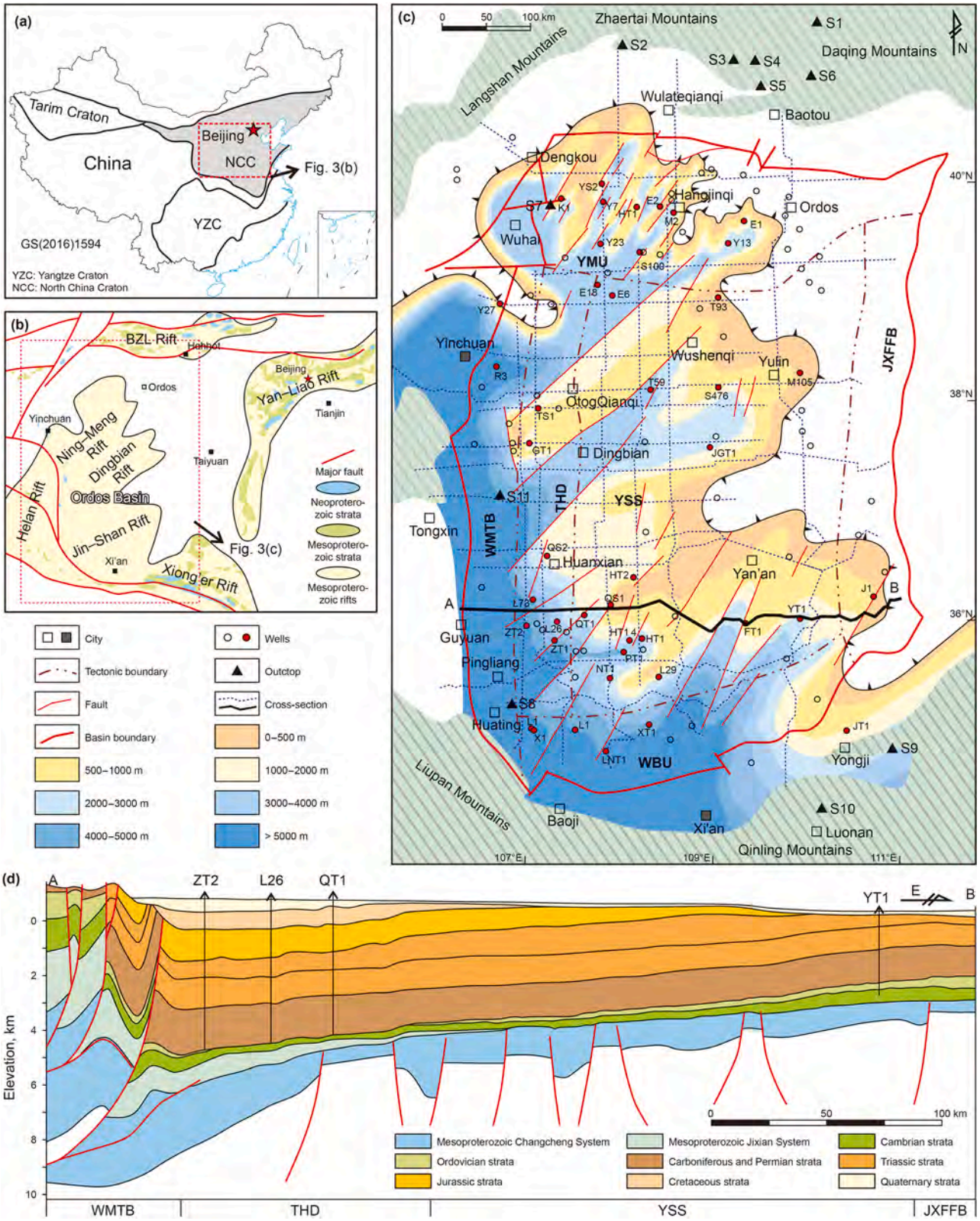

Fig. 3. **(a)** Map showing the location of the North China Craton (NCC) in China, **(b)** the distribution of the Mesoproterozoic rifts and the Meso–Neoproterozoic strata in the NCC (after Li et al., 2019), **(c)** an isopach map of the strata of the Changcheng System, the distribution of the major faults in the Changcheng System, and the locations of the wells, outcrops, seismic profile, cross-sections, and the adjacent orogenic belts in the Ordos Basin, and **(d)** an east–west oriented structural cross-section in the Ordos Basin. The isopach map and structural profile are courtesy of the PetroChina Changqing Oilfield Company. Outcrops: S1: Bayinbulage, S2: Wujiahe, S3: Hewan, S4: Xiaoshetai, S5: Shujigou, S6: Guyang, S7: Mo'ergou, S8: Tongcheng, S9: Zhongtiao Mountains, S10: Luonan, S11: Qinglong Mt. YSS = Yishan slope, THD = Tianhuan depression, YMU = Yimeng uplift, WBU = Weibei uplift, WMTB = Western margin thrust belt, JXFFB = Jinxi fault-fold belt.

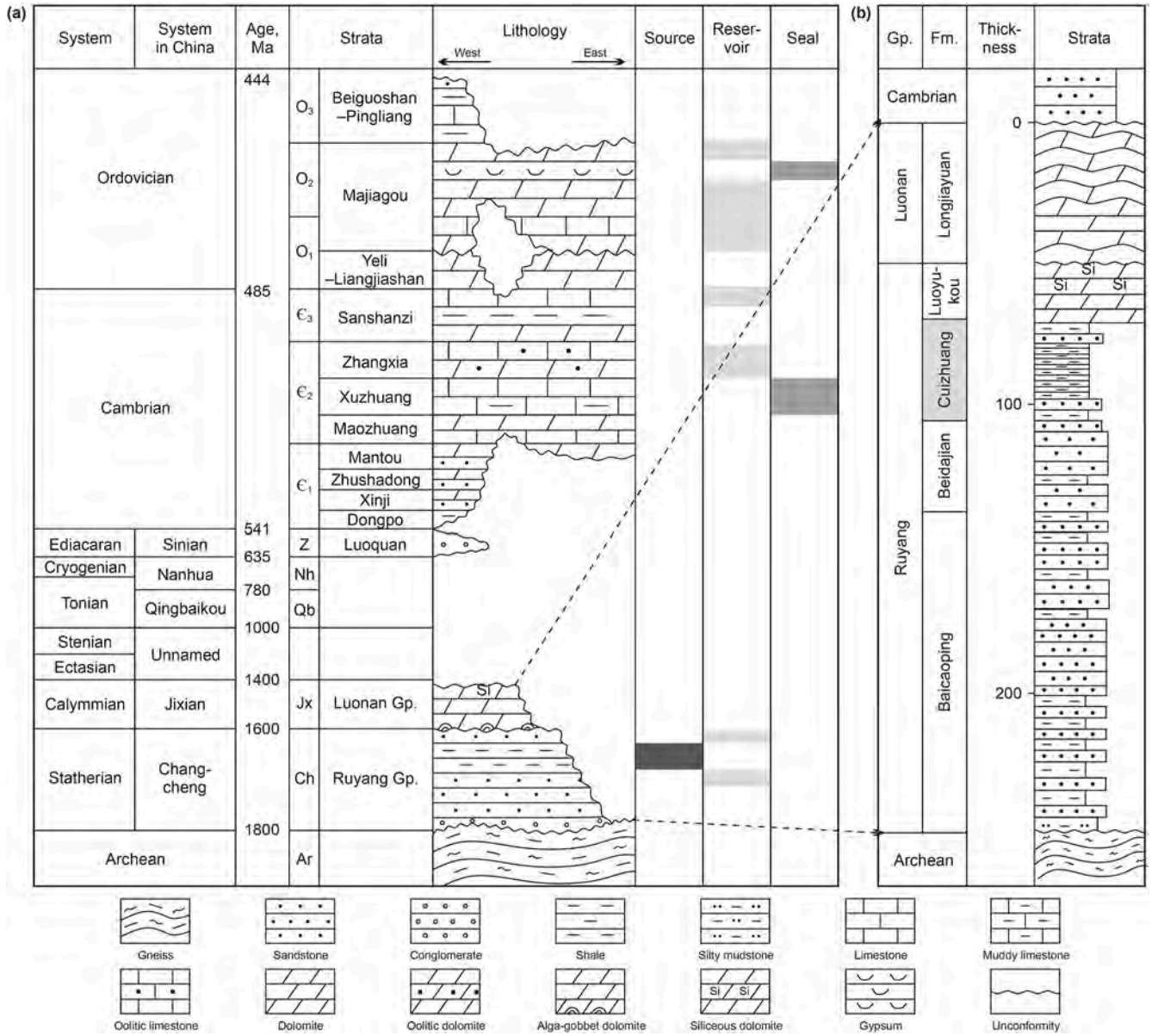

Fig. 4. **(a)** Stratigraphic column and combination of source, reservoir, and seal rocks in the Mesoproterozoic petroleum system in the Ordos Basin, and **(b)** the measured Meso–Neoproterozoic profile in the Zhongtiao Mountains outcrop (after Pan et al., 2020). Gp., Group; Fm., Formation.

potential (Feng et al., 2015, 2020; Guo et al., 2016; Hao et al., 2016; Wang et al., 2018; Zhao et al., 2018; Du et al., 2019; Bai et al., 2020). In the outcrops in the Yinshan area, such as the Guyang, Hewan, Shujigou outcrops, it has been observed that the black shales of the Changcheng System have undergone significant thermal evolution, with R_o values of 2.03%–5.86% and T_{max} values of 556–564 °C. The total organic carbon (TOC) content is mostly between 1.0% and 8.0% but can reach 17.0%. This indicates that these shales are a high-quality hydrocarbon source rock (Table 1). Similarly, the source rocks in the Changcheng System also outcrop in Luonan and the Zhongtiao Mountains in the southern margin. The thermal evolution degree of these source rocks is high, with R_o values of 2.50%–4.40% and T_{max} values of 441–608 °C. However, the TOC content is quite low, with average values of 0.4% and 0.51%, respectively.

Data from typical wells intersecting the Changcheng System source rock within the basin confirm the significant hydrocarbon potential of the Mesoproterozoic strata. For instance, well T59 contains grey-black shale with a total thickness of about 3 m. Its TOC values are about 0.46%, with corresponding R_o values of about 1.8%–2.2% (Zhao et al., 2018). Well PT1 contains two dark shale intervals within the Cuizhuang Formation. The upper interval is 22.5 m thick and has TOC values of 0.07%–0.36%; whereas the lower interval is 5.5 m thick with TOC values of 0.14%–1.47% and R_o values of about 2.6%–2.7%. Well JT1 contains grey-black shale in the lower part of the Cuizhuang Formation, with a thickness of 22 m. Its TOC values are mainly between 0.5% and 0.7% (maximum: 0.95%; average: 0.62%), with R_o values of 2.39%–2.40%. In contrast, the Jixian System is characterized by relatively poor source rocks. In typical wells and the Tongcheng outcrop, it has low TOC values of only 0.08%–0.15% (Table 1).

On a calibrated seismic section, the source rocks in wells T59, PT1 and JT1 correspond to a set of strong seismic reflections. Based on this correlation, the distribution of source rocks in the Changcheng System was mapped across multiple seismic sections. The findings indicate that the source rocks developed in the branched

Table 1
Statistics on basic parameters of the Meso–Neoproterozoic source rocks in the Ordos Basin and its periphery. Data in brackets: averages;/: no data.

Strata	Location of data point	Lithology	TOC, %	R_o, %	T_{max}, °C	Literature
Jixian System	ZT1	Dolomite	0.05–0.18 (0.08)	2.33–2.67 (2.46)	520	PetroChina Changqing Oilfield Company
	NT1	Dolomite	0.08–0.34 (0.15)	/	/	PetroChina Changqing Oilfield Company
	Tongcheng	Dolomite	0.03–0.22 (0.14)	2.7–3.6	505–582	Li et al. (2011)
Changcheng System	T59	Dark shale	(0.46)	1.8–2.2 (2.0)	404–523 (465)	PetroChina Changqing Oilfield Company; Zhao et al. (2018)
	JT1	Dark shale	0.22–0.98 (0.62)	2.39–2.40	/	Du et al. (2019); Bai et al. (2020)
	PT1	Dark shale	0.16–1.47 (0.74)	2.60–2.70	542–554 (549)	PetroChina Changqing Oilfield Company
	Luonan	Slate	0.08–1.52 (0.40)	3.85–4.40 (4.16)	583–601 (590)	Feng et al. (2015); Hao et al. (2016); Wang et al. (2018)
	Zhongtiao Mountains	Slate	0.20–1.21 (0.51)	2.5–3.0 (2.6)	441–608 (520)	Wang et al. (2018); Zhao et al. (2018); Pan et al. (2020)
	Guyang	Slate	0.80–17.0 (3.80)	4.33–5.09	556–564	Zhao et al. (2018); Bai et al. (2020); Feng et al. (2020)
	Bayannuorigong	Slate	(1.83)	2.03–5.86	/	Bai et al. (2020)
	Wujiahe	Slate	(0.86)		/	
	Hewan	Slate	(3.65)		/	
	Shujigou	Slate	(3.50)		/	
	Xiaoshetai	Slate	(2.44)		/	
	Bayinbulage	Slate	(1.56)		/	

rifts are thinner in the Yishan slope (YSS) and Tianhuan depression (THD), with thickness mainly within the range of 5–20 m. In contrast, the source rocks in the Western margin thrust belt (WMTB) and Weibei uplift (WBU) are significantly thicker, reaching more than 30 m thick (Fig. 5).

3.2.2. Mechanism of organic matter enrichment

Trace and rare earth element analysis is commonly used to study ancient depositional environments and mechanism of organic matter enrichment. In this study, we used data from the Zhaertai Group (Changcheng System) in Guyang and Shujigou outcrops (BZL Rift) (Feng et al., 2020, 2024), the Changcheng System in the Zhongtiao Mountains (Xiong'er Rift) (Pan et al., 2020), and the Changcheng System in typical wells within the basin (this study). Among them, the outcrop samples and dark shales from wells PT1 and JT1 are representative of source rocks, whereas the TOC contents of the other samples were less than 0.2%.

Compared with the upper continental crust (UCC) of North China, the contents of V and Ni among the trace elements in most samples from typical wells are relatively high, whereas the contents of Sr and Ba are significantly lower than the background values. The V content is 31.5–170.7 ppm (average of source rock = 97.2 ppm; average of non-source rock = 81.5 ppm; Table 2), and the Ni content is 20.8–66.4 ppm (average of source rock = 29.1 ppm; average of non-source rock = 35.2 ppm). These values are higher than those of the UCC of North China (V: 68 ppm; Ni: 24 ppm) and lower than those of Post-Archean Australian Shale (PAAS) (V: 150 ppm; Ni: 55 ppm). The Sr content is 40.2–132.1 ppm (average of source rock = 83.9 ppm; average of non-source rock = 84.4 ppm), and the Ba content is 150.9–565.4 ppm (average of source rock = 309.4 ppm; average of non-source rock = 360.6 ppm). All of these values are lower than those of the UCC of North China (Sr: 330 ppm; Ba: 740 ppm) and those of PAAS (Sr: 200 ppm; Ba: 650 ppm). The total REE (ΣREE) contents of the shales from typical wells are 48.87–314.21 ppm. Among them, the average value of source rock is 156.7 ppm, and the average value of non-source rocks is 155.8 ppm, both of which are lower than corresponding values for the UCC of North China (174.1 ppm) and that of PAAS (210 ppm). The average value of light REE (LREE) content in

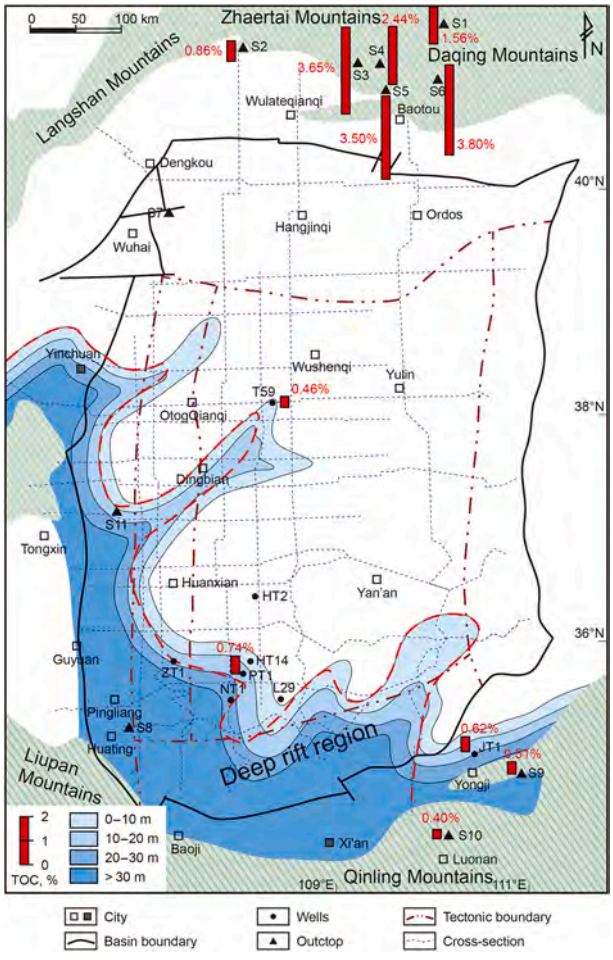

Fig. 5. Map showing the TOC contents in outcrops and typical wells, and thickness of the Mesoproterozoic source rocks in the Ordos Basin and its periphery. The height of the red rectangle and its adjacent numerical value indicate the level of TOC content. The deep rift region containing high-quality source rocks is located to the southwest of the red dashed line. This map is courtesy of the PetroChina Changqing Oilfield Company.

Table 2
Trace and rare earth element data of Changcheng System sediments in the Ordos Basin.

Sample	HT14-01	HT14-02	HT14-03	HT14-04	HT14-05	HT14-06	HT14-07	HT14-08	HT14-09	HT14-10	HT14-11	HT14-12	HT14-13	HT14-14	HT14-15	HT14-16	HT14-17	HT14-18	HT14-19
Depth, m	4713.9	4714.5	4715.6	4717	4717.6	4718.4	4719.4	4720.1	4721.5	4722.3	4723.1	4723.9	4724.6	4725.6	4726.4	4728.7	4803.9	4805.9	4807.7
Lithology	Dark shale	Dark shale	Dark shale	Dark shale	Dark shale	Dark shale	Dark shale	Dark shale	Dark shale	Dark shale	Dark shale	Dark shale	Dark shale	Dark shale	Dark shale	Dark shale	Dark shale	Dark shale	Grey-green shale
Sc	9.40	10.63	13.03	10.30	13.16	13.34	15.61	10.95	12.71	13.21	13.18	14.18	10.39	10.91	13.53	8.28	14.45	14.01	13.61
V	67.88	91.18	87.49	86.39	88.47	83.27	86.19	90.60	101.18	92.79	95.35	95.71	78.60	67.97	55.91	31.53	76.82	72.16	77.20
Ni	26.05	44.59	38.39	34.10	39.02	32.84	35.01	36.83	39.66	40.89	39.80	41.41	35.99	34.30	32.75	28.15	32.75	32.02	32.51
Cu	121.91	32.37	16.27	27.06	12.88	57.60	43.18	20.09	28.95	22.38	22.17	15.43	16.25	2.48	3.01	3.58	1.84	1.64	1.88
Sr	94.53	79.96	90.94	84.35	100.38	119.48	132.11	80.57	102.03	87.80	101.04	96.80	83.01	93.83	104.52	109.75	83.23	96.26	81.25
Zr	257.78	191.71	155.85	178.61	172.83	182.66	189.31	162.42	152.15	134.66	141.62	137.58	168.99	168.63	213.61	286.95	141.73	143.91	134.49
Ba	505.27	386.54	387.76	391.44	438.71	565.44	550.26	371.74	387.17	334.40	373.33	366.82	363.17	392.98	410.63	549.53	324.16	372.07	325.20
La	29.64	23.36	26.74	26.83	31.43	37.05	45.75	22.70	25.00	28.40	31.30	31.11	33.14	41.25	45.05	67.28	36.28	40.92	36.37
Ce	62.56	52.06	61.38	58.98	66.33	79.38	93.56	52.02	55.91	59.17	66.98	64.52	68.37	76.93	85.95	129.07	74.50	79.42	69.20
Pr	7.16	5.97	6.78	6.70	7.61	8.72	10.09	5.92	6.54	7.09	7.80	7.72	7.84	8.95	9.34	13.90	8.68	9.05	8.28
Nd	28.28	23.30	26.51	26.17	29.50	32.28	36.89	23.52	25.94	27.82	29.47	29.45	29.18	31.55	33.85	52.51	32.69	32.69	29.99
Sm	5.27	4.21	4.78	4.70	5.17	6.14	6.92	4.30	4.77	4.86	5.37	5.28	5.13	5.44	6.36	10.16	6.38	6.08	5.66
Eu	1.10	0.81	0.93	0.94	1.01	1.26	1.40	0.87	0.94	0.92	1.03	1.00	1.02	1.05	1.29	2.30	1.23	1.25	1.16
Gd	4.35	3.45	4.19	3.91	4.35	5.13	5.77	3.58	3.90	3.90	4.34	4.30	4.36	4.76	5.88	11.50	5.34	5.14	4.74
Tb	0.62	0.49	0.59	0.55	0.61	0.69	0.78	0.50	0.56	0.55	0.61	0.59	0.60	0.63	0.78	1.72	0.74	0.68	0.65
Dy	3.51	2.90	3.40	3.18	3.53	3.89	4.38	2.93	3.38	3.27	3.58	3.44	3.45	3.54	4.28	10.47	4.13	3.83	3.65
Ho	0.69	0.57	0.66	0.62	0.69	0.74	0.84	0.58	0.67	0.65	0.71	0.69	0.68	0.70	0.82	2.11	0.79	0.73	0.70
Er	2.01	1.68	1.91	1.81	2.00	2.16	2.41	1.70	1.95	1.91	2.09	2.04	2.03	2.08	2.39	5.98	2.25	2.10	2.00
Tm	0.30	0.25	0.29	0.27	0.30	0.31	0.35	0.26	0.30	0.28	0.31	0.31	0.31	0.32	0.36	0.88	0.33	0.31	0.29
Yb	1.99	1.68	1.91	1.77	1.98	2.06	2.28	1.67	1.93	1.86	2.00	1.97	2.05	2.09	2.34	5.52	2.14	1.99	1.89
Lu	0.29	0.25	0.28	0.26	0.29	0.30	0.34	0.25	0.28	0.27	0.29	0.29	0.30	0.32	0.35	0.81	0.32	0.29	0.28
Th	9.72	7.79	9.00	8.58	9.60	10.78	12.29	7.85	8.55	8.65	9.58	9.23	8.83	9.47	10.85	12.88	9.70	11.04	10.06
U	1.47	1.43	1.63	1.33	1.73	1.58	1.82	1.33	1.38	1.25	1.49	1.37	1.26	1.52	1.76	1.71	1.30	1.87	1.32
ΣREE	147.76	120.99	140.36	136.70	154.81	180.12	211.74	120.80	132.06	140.96	155.89	152.70	158.47	179.60	199.05	314.21	175.79	184.50	164.85
LREE	134.01	109.71	127.13	124.32	141.05	164.83	194.59	109.33	119.10	128.26	141.95	139.09	144.67	165.18	181.85	275.22	159.76	169.42	150.66
HREE	13.75	11.27	13.23	12.38	13.76	15.28	17.15	11.47	12.96	12.70	13.94	13.61	13.80	14.42	17.20	38.99	16.03	15.08	14.19
$(La/Yb)_N$	10.06	9.37	9.45	10.20	10.70	12.15	13.55	9.15	8.75	10.30	10.56	10.67	10.88	13.32	12.97	8.21	11.42	13.83	12.97
δEu	0.68	0.63	0.62	0.65	0.63	0.67	0.66	0.66	0.65	0.63	0.63	0.62	0.64	0.62	0.64	0.65	0.63	0.67	0.67
δCe	1.00	1.04	1.07	1.03	1.00	1.03	1.01	1.06	1.03	0.98	1.01	0.98	0.99	0.92	0.96	0.97	0.98	0.95	0.92

Sample	HT14-20	HT14-21	HT2-01	HT2-02	JT1-01	JT1-02	JT1-03	JT1-04	JT1-05	JT1-06	JT1-07	JT1-08	JT1-09	L29-01	L29-02	PT1-01	PT1-02	PT1-03	PT1-04
Depth, m	4809.7	4811.4	4590.1	4591	2086.3	2088.2	2089.9	2091.7	2115.7	2116.5	2118.4	2118.8	2148.8	4423.4	4427.5	4830.4	4831.5	4832.6	4834.1
Lithology	Purple-red shale	Purple-red shale	Purple-red shale	Purple-red shale	Grey-green shale	Purple-red shale	Grey-green shale	Dark shale	Dark shale	Dark shale	Dark shale	Dark shale	Dark shale	Purple-red shale	Purple-red shale	Dark shale	Dark shale	Dark shale	Dark shale
Sc	15.40	13.14	18.77	12.16	10.78	30.30	15.22	18.83	15.34	22.37	11.85	11.03	14.66	7.6341	8.4498	12.72	10.73	12.01	15.64
V	80.79	80.54	151.27	83.63	50.01	98.26	86.33	98.79	96.64	170.65	76.81	64.42	83.58	57.929	67.506	101.71	81.10	101.71	96.59
Ni	33.22	32.44	43.07	66.37	23.18	40.34	27.36	34.85	23.20	27.32	28.05	23.53	26.77	22.63	20.797	33.49	25.24	37.66	30.38
Cu	19.58	1.47	3.58	11.89	11.91	20.79	45.49	9.21	3.89	6.49	3.65	4.41	18.75	2.2266	1.5607	14.22	20.10	20.76	4.46
Sr	93.21	82.11	43.45	51.92	74.82	55.21	48.55	68.40	69.68	73.82	81.50	78.38	81.01	50.929	40.176	97.96	107.64	94.48	86.03
Zr	127.86	132.18	212.08	603.33	122.18	117.76	130.02	146.47	169.36	155.37	165.59	207.90	147.47	57.185	123.42	140.70	294.72	140.61	163.30
Ba	390.41	379.57	276.23	340.77	214.36	159.10	168.16	224.44	222.51	191.00	268.40	266.28	255.65	150.89	221.66	394.98	552.01	351.82	366.47
La	43.33	38.95	17.33	8.37	37.36	21.75	14.36	25.26	31.64	25.78	40.87	24.36	42.86	23.562	36.756	24.05	37.02	29.35	37.46
Ce	83.08	73.31	37.52	19.36	80.94	48.36	41.05	55.93	72.83	60.15	78.00	59.83	84.78	53.354	70.086	58.00	73.34	64.95	73.88
Pr	9.92	8.97	4.84	1.99	8.73	5.20	4.12	6.44	7.92	6.57	9.27	6.25	9.20	5.5779	7.3295	6.34	8.53	7.32	8.66
Nd	37.20	33.29	19.20	7.60	32.36	20.76	15.88	25.94	29.81	26.16	33.38	24.76	32.10	22.135	27.847	25.00	30.81	28.70	32.03
Sm	7.55	6.59	4.21	2.07	6.55	4.17	3.10	4.95	5.84	4.91	5.69	4.86	5.18	4.3206	4.7741	4.44	5.64	5.14	6.32
Eu	1.47	1.27	1.06	0.69	1.42	0.95	0.63	0.97	1.06	1.06	1.06	0.97	0.97	0.8103	0.869	0.84	1.15	0.99	1.22
Gd	5.79	5.26	3.97	2.24	5.83	3.85	2.62	3.95	4.48	4.06	4.48	4.37	4.14	3.8922	4.0628	3.54	4.61	4.21	5.50
Tb	0.74	0.70	0.63	0.37	0.77	0.60	0.40	0.56	0.61	0.59	0.58	0.65	0.55	0.5598	0.5235	0.50	0.64	0.60	0.78
Dy	4.00	3.80	3.80	2.35	4.10	3.50	2.47	3.32	3.53	3.63	3.29	3.92	3.17	3.3093	2.9376	2.91	3.68	3.51	4.52
Ho	0.75	0.72	0.74	0.48	0.76	0.66	0.50	0.65	0.70	0.72	0.64	0.76	0.63	0.6514	0.5796	0.56	0.71	0.68	0.87
Er	2.12	2.04	2.11	1.41	2.08	1.83	1.47	1.88	2.04	2.10	1.90	2.17	1.88	1.8633	1.711	1.64	2.06	1.98	2.50

Tm	0.30	0.30	0.32	0.22	0.30	0.27	0.23	0.28	0.30	0.32	0.29	0.33	0.28	0.2747	0.253	0.25	0.31	0.30	0.38
Yb	1.94	1.90	2.07	1.48	1.89	1.72	1.52	1.88	2.01	2.10	1.89	2.15	1.84	1.7375	1.6264	1.62	2.01	1.91	2.41
Lu	0.28	0.28	0.31	0.24	0.28	0.25	0.23	0.28	0.30	0.32	0.28	0.31	0.27	0.2528	0.2422	0.24	0.30	0.28	0.36
Th	10.89	10.89	4.86	4.69	10.98	6.06	5.49	7.76	8.82	7.14	11.91	9.54	11.41	6.043	11.523	8.01	11.94	9.05	9.68
U	1.53	1.61	1.35	1.40	1.25	0.93	0.93	1.17	1.24	1.47	1.14	1.65	1.28	1.6516	1.9688	1.56	1.79	1.34	2.04
ΣREE	198.49	177.39	98.12	48.87	183.38	113.85	88.57	132.30	163.06	138.48	181.64	135.68	187.86	122.30	159.60	129.94	170.80	149.91	176.88
LREE	182.55	162.39	84.16	40.08	167.37	101.17	79.15	119.49	149.10	124.64	168.28	121.02	175.09	109.76	147.66	118.67	156.48	136.44	159.57
HREE	15.94	15.01	13.96	8.79	16.01	12.68	9.43	12.81	13.96	13.84	13.36	14.66	12.76	12.54	11.94	11.26	14.32	13.46	17.31
$(La/Yb)_N$	15.05	13.79	5.63	3.81	13.32	8.50	6.39	9.06	10.62	8.29	14.55	7.63	15.71	9.14	15.24	10.01	12.41	10.34	10.47
δEu	0.66	0.64	0.78	0.98	0.69	0.71	0.66	0.65	0.61	0.71	0.62	0.63	0.62	0.59	0.59	0.63	0.67	0.63	0.62
δCe	0.93	0.91	0.97	1.11	1.04	1.06	1.27	1.03	1.08	1.09	0.93	1.14	0.98	1.08	0.97	1.11	0.96	1.04	0.95

* $(La/Yb)_N$ is the chondrite-normalized ratios. $\delta Eu = 2Eu_N/(Sm_N + Gd_N)$, $\delta Ce = 2Ce_N/(La_N + Pr_N)$. "N" stands for chondrite-normalization.

source rocks is 142.9 ppm, and that in non-source rocks is 141.2 ppm; the average value of heavy REE (HREE) content in source rocks is 13.8 ppm, and that in non-source rocks is 14.6 ppm. These values are comparable to those of the UCC of North China (LREE = 144.1 ppm; HREE = 12.97 ppm), and lower than those of PAAS (LREE = 165.6 ppm; HREE = 17.4 ppm).

The chondrite-normalized REE patterns of shales in Changcheng System are relatively consistent (Fig. 6), characterized by enrichment of LREEs and depletion of HREEs, exhibiting distinct upper crustal characteristics. The ΣREE fractionation index $(La/Yb)_N$ values of source rocks range 7.63–15.71, with an average of 10.91 (the UCC of North China = 12.42; PAAS = 9.15), indicating a significant REE and LREE fractionation. The δEu values is 0.61–0.71, with an average of 0.64, indicating a negative anomaly and the absence of hydrothermal activity. The δCe values range 0.93–1.14, with an average of 1.03, showing marginally negative or positive anomaly, which suggest continuous anoxic conditions in the surface-water, that restricted the evolution of eukaryotes and limited the productivity of the Changcheng System (Tang et al., 2016).

3.2.2.1. Sedimentary provenance. Sedimentary provenance can be determined using the Th/Sc–Zr/Sc plot, which shows that the compositions of the source rocks plot along the basalt–felsic volcanic rock–granite (B–F–G) line (Fig. 7(a)). The source rocks in the northern outcrops are compositionally biased toward a granitic source, whereas those in the southern outcrops tend toward a basaltic source. The compositions of source rocks in typical wells within the basin are intermediate between these two end-members. Although a mafic provenance provided more abundant nutrients (Cox et al., 2016), the source rocks with higher TOC contents in the northern outcrops are biased toward a felsic source. This suggestes that the sedimentary provenance may not have been the primary factor controlling the formation of the Changcheng System source rocks.

3.2.2.2. Paleoclimate and paleosalinity. The Sr/Cu ratio is an effective indicator of paleoclimate. Generally, Sr/Cu ratios <10.0 indicate a humid climate, while ratios >10.0 signify an arid climate (Fan et al., 2024). The source rocks in the southern outcrops yield Sr/Cu ratios of 0.2–23.0 (average 4.89), and those in the northern outcrops yield ratios of 0.46–21.58 (average 8.11), indicating a warm and humid climate overall. In contrast, the source rocks in typical wells within the basin have Sr/Cu ratios of 4.3–22.3 (average 11.7), signifying a relatively arid climate (Fig. 7(b)). These results reveal that the paleoclimate during deposition of the Changcheng System source rocks varied spatially, transitioning from warm and humid conditions in the marginal outcrops to relatively arid conditions in the basin interior.

Paleosalinity is a crucial parameter for assessing depositional environments associated with source rocks. Th/U ratios >7 indicate a terrestrial freshwater environment, ratios of 2–7 indicate a brackish sedimentary environment, and ratios <2 indicate a marine saline environment (Fu et al., 2018). The Th/U ratios of the source rocks in the southern outcrops range from 4.92 to 8.98 (average 6.63); those in the northern outcrops range from 1.26 to 4.72 (average 3.16); and those in typical wells within the basin range from 4.75 to 10.41 (average 6.7). It can be inferred that the source rocks from the southern outcrops and typical wells within the basin were likely deposited in a nearshore brackish sedimentary environment with significant terrigenous input, whereas those from the northern outcrops were predominantly formed in a neritic sedimentary setting characterized by moderate salinity.

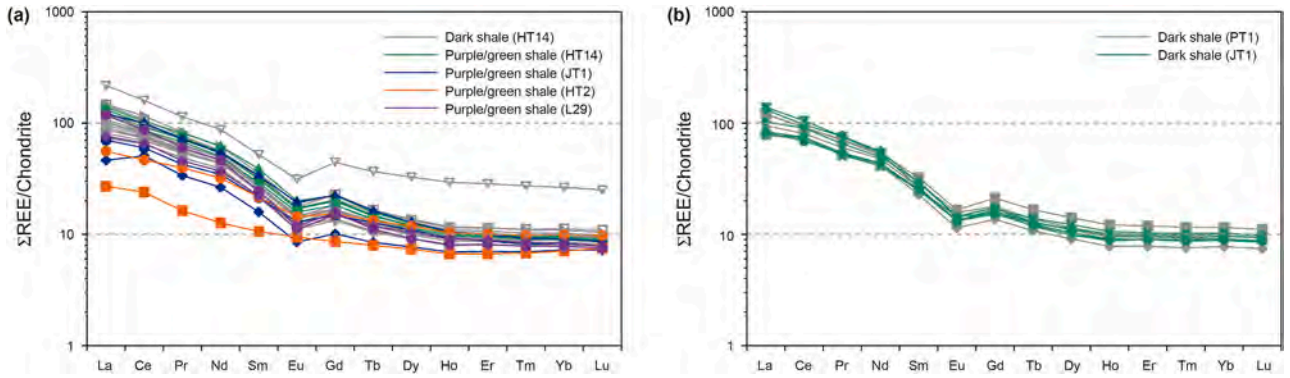

Fig. 6. Chondrite-normalized REE distribution patterns of shales in Changcheng System from typical wells within the Ordos Basin. **(a)** Samples of non-source rocks from wells HT14, JT1, HT2, and L29; **(b)** samples of source rocks from wells PT1 and JT1.

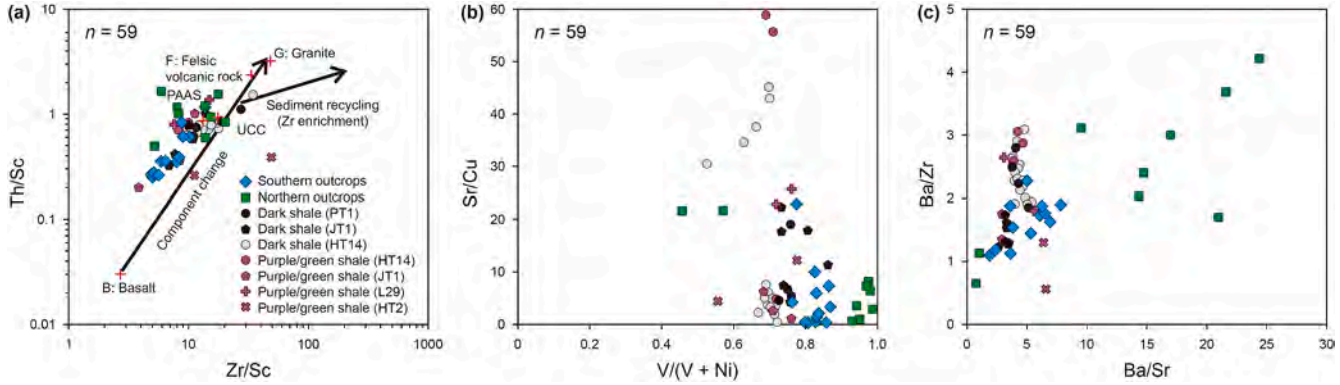

Fig. 7. **(a)** Th/Sc verses Zr/Sc plot for determining the sedimentary provenance, **(b)** plot of Sr/Cu versus V/(V + Ni) for determining the sedimentary environment, and **(c)** Ba/Zr versus Ba/Sr plot for determining the submarine hydrothermal conditions for the Mesoproterozoic shales. See text for discussion. The data for the southern and northern outcrops are from Feng et al. (2020, 2024) and Pan et al. (2020).

3.2.2.3. Basin redox conditions. Redox conditions are another crucial factor during the formation of source rocks. It is widely accepted that V/(V + Ni) ratios <0.46 indicate oxic conditions, ratios of 0.46–0.6 indicate dysoxic conditions, and ratios >0.6 indicate anoxic conditions (Hatch and Leventhal, 1992; Rimmer, 2004). The V/(V + Ni) ratios of the source rocks in the southern outcrops are 0.76–0.87, with an average of 0.82; those in the northern outcrops are 0.46–0.99, with an average of 0.86; and those in typical wells within the basin are 0.73–0.86, with an average of 0.76 (Fig. 7(b)). These values indicate that the source rocks were predominantly deposited under anoxic bottom-water conditions. The positive correlation between V and TOC content further suggests that anoxic conditions favored the preservation of organic matter in these strata (Pan et al., 2020).

3.2.2.4. Paleoproductivity. The geochemical behaviors of Zr and Sr are analogous to those of SiO_2 and $CaCO_3$, that is, Zr can serve as an indicator of terrigenous input, whereas Sr is a biophile element and a proxy for non-terrigenous deposits. Ba in marine sediments can be derived from multiple sources, including biogenic barium, terrigenous silicates, submarine hydrothermal fluids, and secretions from benthic organisms (Schmitz, 1987). Consequently, the Ba content of marine sediments reflects the biological flux from the overlying water column, thereby serving as a proxy for paleoproductivity (Dean et al., 1997; McManus et al., 1999). The Ba/Zr ratios of the source rocks in the southern outcrops are 1.1–2.3, with an average of 1.6; those in the northern outcrops are 0.7–4.2, with an average of 2.4; and those in typical wells within the basin are 1.2–2.8, with an average of 1.8 (Fig. 7(c)). These results indicate that the paleoproductivity of the southern outcrops was similar to that within the basin but was significantly lower than that of the northern outcrops. Furthermore, the Ba/Sr ratio can be used as a scale for measuring submarine hydrothermal activity, that is for marine sediments, higher Ba/Sr ratios indicate a stronger degree of influence by submarine hydrothermal activity (Magenheim and Gieskes, 1992; Chen et al., 2004). The Ba/Sr ratios of the source rocks in the southern outcrops are 1.9–7.8, with an average of 5.0; those in the northern outcrops are 0.7–24.4, with an average of 13.8; and those in typical wells within the basin are 2.6–5.1, with an average of 3.6 (Fig. 7(c)). These results indicate that submarine hydrothermal activity was likely the primary factor contributing to the high paleoproductivity in the northern outcrops as it could bring abundant nutrients for the formation of organic matter (Wang et al., 2006).

The organic matter enrichment in the southern outcrops and the typical wells within the basin is primarily controlled by the redox conditions of the bottom water, and it belongs to the preservation-type source rock. The combined effects of a felsic source provenance, a seasonal climatic transition from warm and humid to relatively arid conditions, a nearshore brackish sedimentary environment, and the absence of submarine hydrothermal activity contributed to low primary productivity, resulting in relatively low TOC content in the Changcheng System. In contrast, source rocks in the northern outcrops exhibit higher TOC values under a similar sedimentary setting, which can be attributed to the influence of submarine hydrothermal activity. The submarine hydrothermal activity and anoxic bottom water may have promoted the development of better source rocks in the Changcheng System (Pan et al., 2020). The deep rift region was conducive to forming and preserving better source rocks as it was prone to creating

euxinic-anoxic deep-water conditions and to the occurrence of frequent submarine hydrothermal activity. Therefore, it is speculated that high-quality hydrocarbon source rocks were formed in the deep rift strata of the Baicaoping and Zuizhuang formations.

3.3. Reservoir rocks

3.3.1. Development characteristics of reservoir rocks

During the Changcheng Period, the basin progressively shallowed from the southwest to the northeast, resulting in the successive development of semi-deep marine, neritic, littoral, and deltaic facies (Bai et al., 2022). In the Hangjinqi area, sufficient provenance material and near-provenance accumulation occurred due to its proximity to the Wulangere basement uplift. As a result, fluvial-deltaic deposits with poor reservoir quality developed, including extensive thick sandstone deposits and locally visible bottom conglomerate deposits. Littoral–neritic facies broadly developed in the middle of the basin are predominantly composed of purple-red and grey-white quartz sandstone and lithic quartz sandstone.

The diagenesis of the Changcheng System was relatively complex, including strong compaction (Fig. 8(a)), clay mineral diagenesis (Fig. 8(b) and (c)), siliceous cementation (Fig. 8(d)), calcite cementation (Fig. 8(e)), and dissolution (Fig. 8(f)). Observations of outcrops in Mo'ergou, Zhongtiao Mountains, and Luonan and cores from typical wells in the basin revealed that the reservoir space in the Changcheng System reservoir rocks is primarily composed of primary pores, as well as a small number of solution pores. The reservoir quality of the Changcheng System sandstones is visibly influenced by the sedimentary facies, and the reservoir quality of the littoral–neritic facies is the highest, followed by the fluvial-deltaic facies and semi-deep marine facies. When considering diagenesis, littoral–neritic facies reservoir rocks can be further classified into three types: quartz sandstones characterized by pore-lining clay and microcrystalline quartz (QSPC), quartz sandstones displaying multi-stage siliceous cementation (QSSC), and lithic quartz sandstones with a small number of solution pores (LQS).

The formation and preservation of the primary pores was crucial to the formation of the QSPC reservoir rocks in the Changcheng System, and this process was controlled by the structural and compositional maturity as well as diagenesis. As shown in Fig. 8(b), the lithic quartz sandstone has a low structural maturity, resulting in the scarce development of primary pores and consequently a low reservoir quality. The high compositional maturity, as well as the presence of pore-lining clay and microcrystalline quartz formed after the partial dissolution of feldspar and lithic grains under the leaching effect of early meteoric water (Fig. 8(c)), increased its resistance to compaction, hindered grain contact, restricted cementation, and created a closed condition with overlying thick layers of tight carbonatite, promoting the development of better reservoir rocks. For example, the porosities of the rocks in wells M105 and JGT1 can reach more than 10%.

The multi-stage development of siliceous cementation was the primary factor for the formation of QSSC reservoir rocks. Particularly in the late stage, quartz secondary enlargement exhibited larger crystal sizes and filled both intergranular pores and dissolved pores in grains (Liu et al., 2024). In the central-eastern regions of the basin, the homogenization temperature of fluid inclusions during the early quartz cementation was 83–129 °C, while those during late quartz cementation ranged 156–172 °C (Liu et al., 2024). In the well GT1, located in the central-western parts of the basin, the homogenization temperature of fluid inclusions during the early quartz cementation was 113–158 °C, while those during late quartz cementation ranged 172–183 °C (PetroChina Changqing Oilfield Company). It can be inferred from the burial history that the quartz enlargement in the late stage primarily formed during J_3–K_1. During this period, the source rocks had already entered the gas-generating stage, meaning that these rocks could potentially serve as high-quality reservoir rocks before the Late Jurassic.

The formation of the LQS reservoir rocks was related to the feldspar and lithic grains. Multiple stages of acidic fluid input dissolved the feldspar and lithic grains and formed intragranular solution pores, which improved the physical properties of the Changcheng System to some extent. For example, the porosities of the rocks in well K1 range 1.9%–9.4%, with an average of 5.6%.

Overall, although the Changcheng System tends to be composed of tight sandstone, it also contains effective reservoir rocks with favorable physical properties. Compaction, clay matrix, and quartz secondary enlargement were the main factors of the reservoir densification, while pore-lining clay and feldspar dissolution were the constructive diagenetic properties. As a result, the high structural and compositional maturity (littoral–neritic facies) and the development of pore-lining clay or the occurrence of feldspar dissolution have led to the development of favorable reservoir rocks.

During the Jixian Period, the basin was mainly a marginal depression with a narrow sedimentary range. In this depression, ocean trough, sub-tidal zone, and intertidal zone environments developed from west to east (Bai et al., 2022). The main characteristic of the Jixian System was the development of siliceous material, which can be divided into lamellae, bands, concretions, and scattered patches based on their occurrence forms (Fig. 8(g) and (h)). Microscopic observation of thin sections revealed the presence of abundant primary and secondary pores within the Jixian System. However, the majority of these pores are filled with siliceous cement, resulting in the residual porosity being dominated by moldic pores and microfractures, as well as a small number of locally visible solution pores (Fig. 8(i)). Overall, the matrix of the Jixian siliceous dolomite is tightly cemented. The residual intercrystalline pores, solution pores, and microfractures serve as the reservoir space; however, the reservoir quality is poor and exhibits strong heterogeneity.

3.3.2. Distribution characteristics of reservoir rocks

The reservoir quality of the Changcheng System was influenced by multiple factors, including sedimentary facies, early-stage weathering and leaching (pore-lining clay and microcrystalline quartz), mid-to-late-stage acidic dissolution, and late-stage quartz cementation. Based on this, the reservoir rocks were divided into four types according to the sedimentary facies and stratigraphic contact relationship, as well as diagenetic type. Type I consists of the littoral–neritic facies in the central region of the basin, which has experienced strong weathering and erosion (Ch/∈ unconformity), with an average porosity of 8.26% and an average permeability of 0.7 mD. Locally, reservoir rocks exhibited late-stage quartz cementation, which remained high-quality reservoir rocks during the T–J. Type II consist of the littoral–neritic facies in the southern and northern regions of the basin. It has experienced strong weathering and erosion (Ch/∈ unconformity), and the high content of feldspar and lithic grains facilitated multiple stages of acidic dissolution due to sufficient provenance material, resulting in an average porosity of 6.26% and an average permeability of 0.36 mD. The littoral–neritic facies reservoir rocks that have not experienced weathering and erosion were inferred to belong to type III, due to the scarcity of core samples. Type IV consists of fluvial-deltaic facies, with the porosity mainly ranging 4.2%–6.3%, and the permeability generally within 0.02–0.3 mD.

As shown in Fig. 9, this section presents the reservoir classification within the DB Rift. The Baicaoping Fm. gradually thins eastward, exhibiting a wedge-shaped characteristic of a half-graben structure. Type IV reservoir rocks of fan-delta facies are developed near the

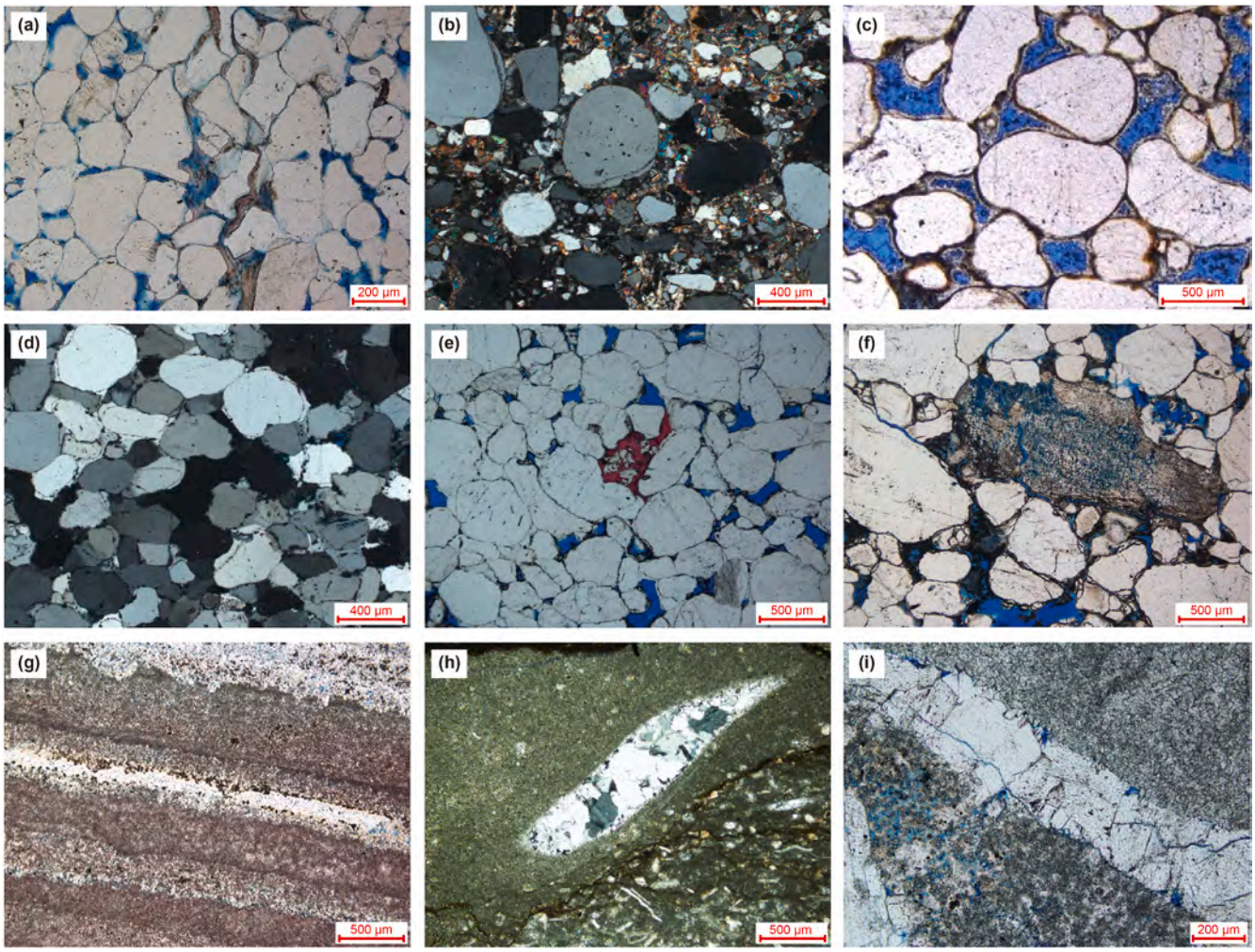

Fig. 8. Types of reservoir spaces and diagenesis of the Mesoproterozoic reservoir rocks. **(a)** Particle line contact in quartz sandstones at 3690.5 m (Ch) in well M105 (−); **(b)** rich clay matrix in lithic quartz sandstone at 3553.8 m (Ch) in well T93 (+); **(c)** pore-lining clay in quartz sandstone at 4175.14 m (Ch) in well JGT1 (−); **(d)** rich quartz secondary enlargement in quartz sandstone at 3758.7 m (Ch) in well S476 (+); **(e)** small amount of calcite cementation (red stained) in quartz sandstone at 3692.9 m (Ch) in well M105 (−); **(f)** intragranular solution pores in quartz sandstone at 3693.5 m (Ch) in well M105 (−); **(g)** algal-laminated siliceous dolomite at 5355.6 m (Jx) in well L73 (−); **(h)** siliceous concretion in dolomite at 5145.1 m (Jx) in well ZT2 (+); and **(i)** solution pores and siliceous bands in dolomite at 5359.2 m (Jx) in well L73 (−). The blue epoxy resin visible in the images indicates the location and distribution of pores. The figure annotations specify that "(−)" denotes observations made under plain-polarized light, whereas "(+)" denotes observations made under cross-polarized light.

faults and gradually transition eastward into the non-reservoir rocks of semi-deep marine facies. The source rocks of the Baicaoping Fm. can develop within these non-reservoir rocks. Continuing eastward, the formation gradually transitions into type III reservoir rocks characterized by littoral–neritic facies. The Beidajian Fm. unconformably overlies the Baicaoping Fm., and it developed littoral–neritic facies characterized by continuous weak reflection on the seismic profile. Due to intense weathering and erosion in the Beidajian Fm., its upper part comprises type I reservoir rocks, while the lower part consists of type II reservoir rocks.

In the Baicaoping Fm., semi-deep marine facies developed in the WMTB and western part of the WBU and extended to the YSS in a finger-shaped pattern, which are non-reservoir rocks. The littoral–neritic facies were deposited in the northeast region of the semi-deep marine facies. Type III reservoir rock developed in the southern part, as it did not experience significant weathering and erosion. Type IV reservoir rock (fluvial-deltaic facies) developed in the northern part. Types I and II reservoir rocks are distributed in wellblocks K1–S100 (Fig. 10(a)). The Beidajian Fm. developed mainly in the central and southern parts of the basin. Semi-deep marine facies developed in the Pingliang–Well XT1 area and west of Dingbian and are non-reservoir rocks. Regarding the littoral–neritic facies, type I reservoir rock is distributed in the eastern area of Dingbian due to the strong weathering and erosion in this area, while the other areas contain type III reservoir rock. The fluvial-deltaic facies deposited near the central pinch-out line are classified as type IV reservoir rock (Fig. 10(b)). The Cuizhuang Fm. Is primarily developed in the southern part of the basin. The littoral–neritic facies deposited in the L73–NT1–FT1 wellblocks are type III reservoir rocks, and the semi-deep marine facies developed in the southern part of these wellblocks are classified as non-reservoir rocks. In addition, there are a few type II reservoir rocks to the east of Yan'an (Fig. 10(c)). The Luoyukou Fm. also developed mainly in the southern part of the basin. The semi-deep marine facies was deposited in the WBU, while the littoral-neritic facies developed in the southern part of Huanxian and Yan'an, and the types II, I, and III reservoir rocks developed successively from east to west (Fig. 10(d)).

3.4. Seals, faults, and traps

From a lithofacies perspective, the regional caprocks in the Mesoproterozoic petroleum system can be categorized into four

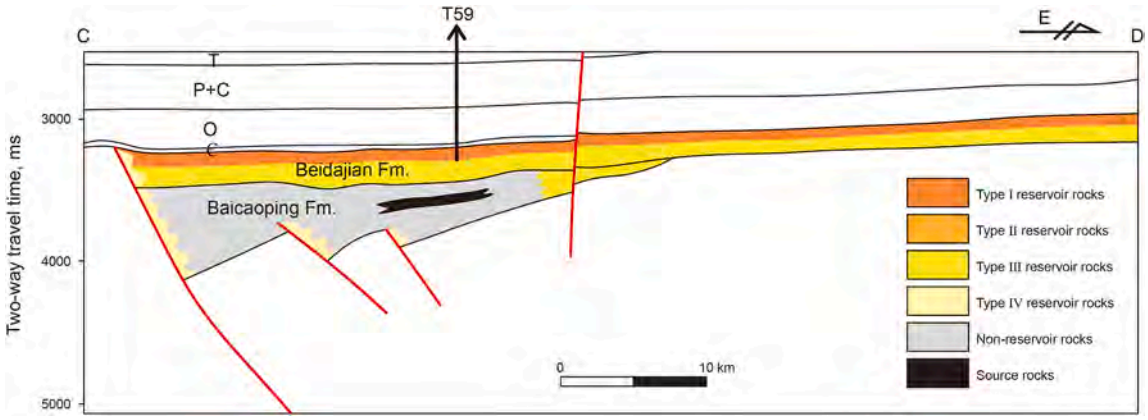

Fig. 9. The filling model of reservoir rocks in the Changcheng System of the DB Rift, Ordos Basin. The cross-section location is shown in Fig. 10(a).

types: tight carbonatite seals, marine shale seals, evaporite seals, and coal measure seals. From a stratigraphic perspective, they can be further divided into Cambrian, Ordovician, and Carboniferous–Permian seal rocks.

The Cambrian seal rocks are primarily comprised of marine shale and tight carbonatite, which has possibly acquired the ability of sealing natural gas since the early Late Triassic (Yuan et al., 2024). The clastics–mixed deposits–carbonates transition was completed during the Mantou–Maozhuang–Xuzhuang period. During this period, the shelf and slope shales with good sealing capabilities developed widely in the western and southern parts of the basin. In the inner part of the basin, the tight carbonatite within the transgressive systems tract is a typical seal rock. These rocks are composed of marl, micrite, dolomicrite, and argillaceous dolomite, are abundant in organic matter, have high mud contents, and are fine in crystalline structures. However, the Cambrian seal rocks are missing in the L73–X1–XT1–QT1 wellblocks, as well as in the northern part of the basin (Fig. 11). The Ordovician seal rocks primarily consist of marine shale and evaporite. The marine shales are primarily distributed in the WMTB. In this area the lithological association of limestone, argillaceous limestone, and argillaceous limestone with a thin layer of shale in the Upper Ordovician Pingliang Fm. and Beiguoshan Fm. provides good sealing capability. The gypsum and salt rocks, which can be divided into several sets—including the first, third, fourth, and fifth members of the Majiagou Fm.—are mainly developed in the Yan'an–Yulin–Ordos area, and have excellent sealing capabilities due to their plastic flow and strong crack healing capability. However, the Ordovician seal rocks are absent in the Hangjinqi–Dingbian–Well XT1 area (Fig. 11). The Carboniferous–Permian coal measure seal rocks are generally developed in the basin and have good sealing capabilities. These seal rocks are comprised of the coal-bearing clastic rock and marine carbonatite in the Carboniferous Benxi Fm. and the Permian Taiyuan Fm. and Shanxi Fm. The thickness of the shales is 80–140 m, the thickness of the coal seams is 4–20 m, and the thickness of the micrites is 8–25 m.

In the regional rift setting in the Ordos Basin, during the Changcheng Period, wide rift troughs with a zonal distribution developed, and listric and composite graben-type faults developed in the NE–SW direction. These faults were further inherited and superimposed in the Caledonian and Hercynian periods and were even reworked and reversed in the Indosinian–Himalayan period, forming a complex fault system in the Mesoproterozoic (Fig. 11). This complex fault system provided pathways for hydrocarbon migration to high parts of the Cambrian and Ordovician strata in the Changcheng System by linking the source rocks in the WMTB, WBU, THD, and YSS.

At present, the top surface of the Changcheng System exhibits a west-dipping monoclinal structure that is high in the east and low in the west. It contains nine rows of nose-uplift structures. Among them, five rows are developed in the NE–SW direction in the northern part of the basin, and four are distributed in the nearly E–W direction in the southern part of the basin. These nose-uplift structures have closure heights of 50–350 m, widths of 20–80 km, and a maximum extension distance is 300 km.

3.5. Evidence of hydrocarbon accumulation

A significant amount of evidence indicates that hydrocarbon migration has occurred in the Meso–Neoproterozoic cores and outcrops within the Ordos Basin. As shown in Fig. 12, abundant solid bitumen is distributed within the fractures in the Jixian System of Qinglong Mountains outcrop, located on the southern margin of the Ordos Basin (Fig. 12(a)). However, due to the tight reservoir rock in this outcrop, no paleo-reservoir was formed. Paleo-reservoir bitumen is distributed in the Jixian System of Tongcheng outcrop, located on the southwestern margin of the Ordos Basin. Abundant solid bitumen is concentrated within an area of over 400 m^2. It is distributed in a laminar form on rock bed surfaces and the inner walls of solution pores and also fills fractures in vein-like shapes (Fig. 12(b)). The pores are half-filled with solid bitumen (Fig. 12(c)). The reflectance of the bitumen R_b is 2.7%–3.6%, exhibiting strong characteristics of pyrobitumen (Li et al., 2011). Similarly, abundant bitumen and hydrocarbon fluid inclusions were found in cores and outcrops of the Changcheng System. For example, the sandstone of the Zhongtiao Mountains exhibits orange and brown fluorescence (Fig. 12(d)), the light-brown sandstone in well T59 exhibits orange and brown fluorescence (Fig. 12(e)), and the hydrocarbon fluid inclusions in the flesh-colored sandstone in well GT1 exhibit blue-white fluorescence (Fig. 12(f)).

Gas chromatography/mass spectrometry GC/MS analysis of the saturated hydrocarbons in chloroform bitumen A from the bitumen in the Jixian System in Tongcheng and the Qinglong Mountains revealed that the saturated hydrocarbons in the two outcrops have a high degree of compositional similarity. The *n*-alkane components of the chloroform bitumen A both exhibit a unimodal distribution, indicating that the source rocks have a single biogenetic composition. The carbon numbers range from nC_{11} to nC_{35}, with a main peak at nC_{23}. The odd-even predominance (OEP) is insignificant, with an average of 0.95. The average Pr/Ph value is 0.8, suggesting a restoring environment. The mass chromatograms for $m/z = 191$ reveal that the bitumen is rich in pentacyclic triterpanes, dominated by C_{30} hopane, and the average

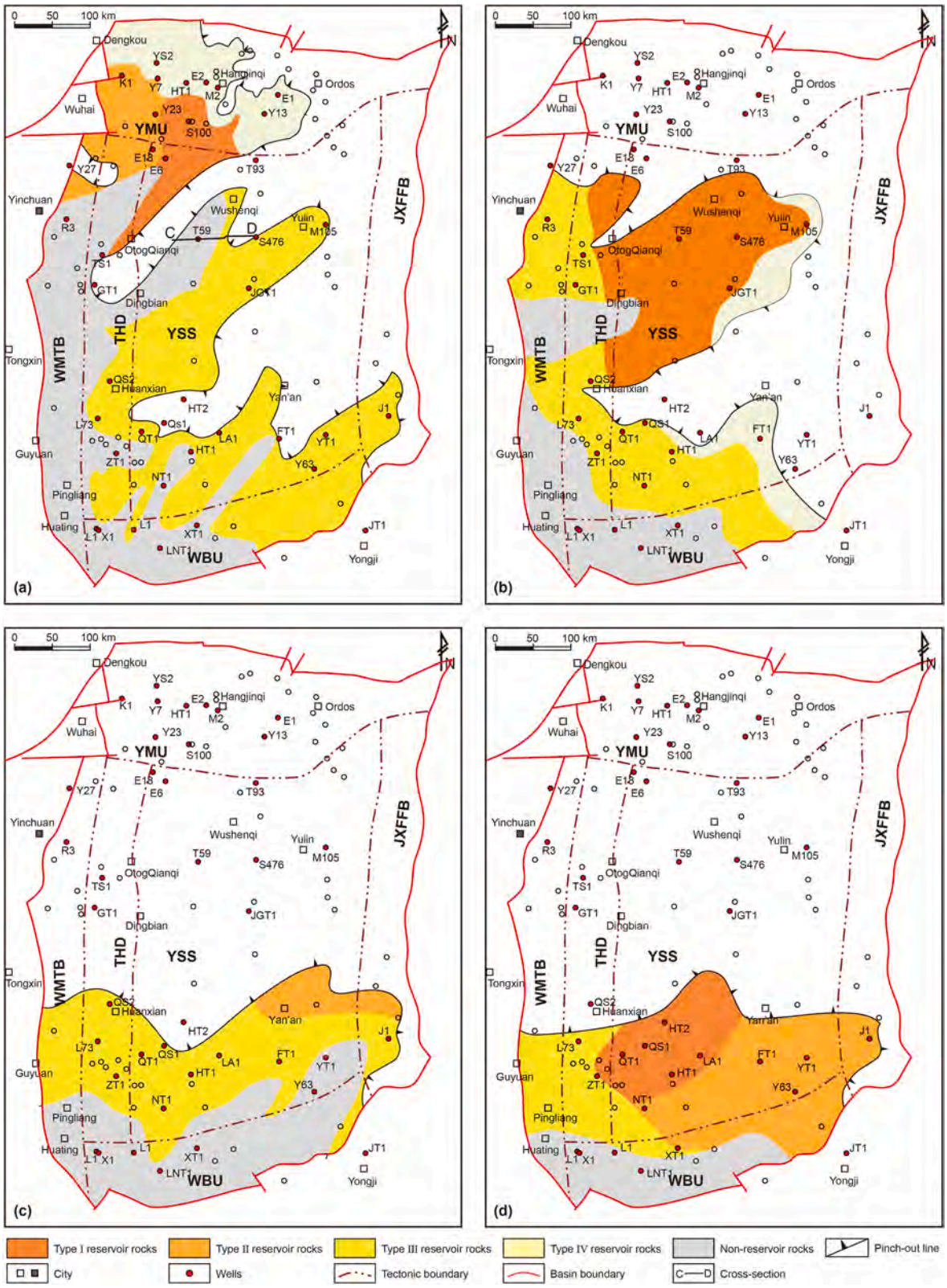

Fig. 10. Distribution of the reservoir rocks in the Changcheng System in the Ordos Basin (after Bai et al., 2020, 2022). **(a)** Baicaoping Fm., **(b)** Beidajian Fm., **(c)** Cuizhuang Fm., and **(d)** Luoyukou Fm.

gammacerane index is 0.17, suggesting that the organic matter was primarily contributed by blue-green algae, bacteria, and other prokaryotes. The bitumen contains a small amount of tricyclic terpanes (TT), with $C_{20}TT < C_{21}TT < C_{23}TT$, and the average Ts/Tm value is 1.24. The mass chromatograms for $m/z = 217$ show that the bitumen is rich in pregnanes. The homohopane $C_{31}22S/(22R + 22S)$ ratio is about 0.6, while the average regular sterane $C_{29}20S/(20R + 20S)$ ratio is only 0.33 which may be attributed to the

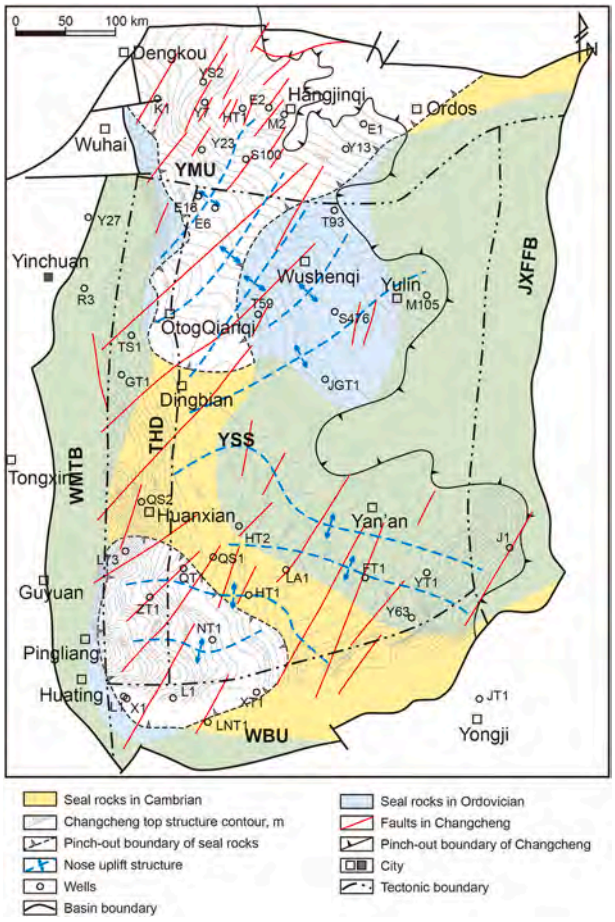

Fig. 11. Distribution of Cambrian and Ordovician seal rocks, structural map of the top surface of the Changcheng System, and the distribution of the major faults in the Changcheng System in the Ordos Basin. This figure is courtesy of the PetroChina Changqing Oilfield Company.

strong biodegradation (Zhu and Zhou, 2018). The parameters of OEP, Ts/Tm and $C_{31}22S/(22R + 22S)$ indicate that the bitumen has experienced a high to over-mature evolution stage (Table 3 and Fig. 13).

The differences in the characteristics of the saturated hydrocarbons in samples from Tongcheng and the Qinglong Mountains are primarily reflected in the contents of the regular C_{27}, C_{28}, and C_{29} steranes. Although both exhibit V-shaped patterns, the content of the C_{27} sterane in the Tongcheng outcrop is higher than that of the C_{29} sterane, while the content of the C_{27} sterane in the Qinglong Mountains outcrop is lower than that of the C_{29} sterane (Fig. 13). The preponderance of the C_{29} sterane may come from planktonic green algae, and C_{27}/C_{29} sterane ratios of >1.0 indicate a neritic environment, while values of <1.0 indicate a deep-water environment (Meng et al., 2006). The biomarker characteristics of the solid bitumen in the Jixian System in Qinglong Mountains are highly consistent with those of the bitumen A extracted from the source rock in the Cuizhuang Fm. In Zhongtiao Mountains, which has a predominance of the C_{29} sterane (Pan et al., 2020). Similarly, the biomarker characteristics of the solid bitumen in the Jixian System in Tongcheng are highly consistent with those of the bitumen A in the Baicaoping Fm. In well T59, with a predominance of the C_{27} sterane. Furthermore, the organic carbon isotope values of solid bitumen in the Tongcheng outcrop range from −14.3‰ to −23.2‰, whereas those of dolomite are −27.6‰, indicating that this is not a near-source accumulation (PetroChina Changqing Oilfield Company). These findings indicate that the bitumen in the outcrop of the Jixian System may have been primarily derived from the source rock in the Changcheng System.

4. Numerical model selection and calibration

4.1. Three-dimensional basin modeling

For the nested simulation of local grid refinement, it was essential to establish a 3-D geological model at the petroleum system scale (basin scale), which provided an ideal solution to simulate the source rock maturation and the hydrocarbon generation and expulsion (Bora and Dubey, 2015). The interest interval for this simulation included the Changcheng System, Jixian System, Cambrian, and Ordovician strata. Based on data availablity and the tectonic evolution stages of the Ordos Basin, 11 sets of sedimentary strata (Ch–Q) were divided into 36 simulation stages, corresponding to seven erosion events and 29 sedimentary events (Table 4). The isopach maps of these stratigraphic units were obtained from the PetroChina Changqing Oilfield Company and published literature (Peng and Wu, 2006; Chen, 2007; Yang et al., 2012a). Furthermore, over 100 wells were calibrated for key layers such as the Cambrian, Ordovician, Permian, Triassic, and Jurassic strata. Erosion maps for four major uplift and erosion events since the Mesozoic (Late Triassic, late Middle Jurassic, Late Jurassic, and Late Cretaceous) were created based on Chen et al. (2006). Erosion maps for the Late Cambrian and Late Ordovician were estimated based on paleogeomorphology data provided by the PetroChina Changqing Oilfield Company. The erosion thickness of the Proterozoic strata was difficult to determine due to their considerable age; therefore, an average value of 500 m was ultimately adopted.

A 3-D conceptual geological model at the basin scale was constructed based on the parameters described above, with a spatial grid resolution of 10 km × 10 km. A lithologic model was also established, incorporating parameters such as grain density, initial porosity, compaction coefficient, permeability, and sedimentary facies. The lithological assignment was simplified according to the sedimentary facies distribution. In this study, the lithofacies and paleogeography of the Upper Paleozoic strata were obtained from Li et al. (2020), while those for the Jixian System–Ordovician were provided by the PetroChina Changqing Oilfield Company.

The source rock model controls hydrocarbon generation, and its key parameters include the effective thickness of the source rock, TOC, hydrogen index (HI), organic facies, and a kinetic model for the hydrocarbon generation. The source rocks in the southern part of the basin are primarily developed in the Cuizhuang Formation, while those in the northern part of the basin are primarily distributed in the Baicaoping Formation. Accordingly, the source rocks were assigned to their respective strata, and the organic facies were divided into deep rift facies and margin rift facies. Due to the limited availability of source rock samples and the relatively low restitution coefficient of low-organic-matter source rocks (Qin et al., 2007), the TOC and HI values in the deep rift region were set to 2.0% and 500 mg/g, respectively, while those in the margin rift region were set to 0.6% and 400 mg/g, respectively. Additionally, the Pepper and Corvi's (1995) Type I (C) kinetic model was selected because type I kerogen is prevalent in the source rocks of the Changcheng System.

Although the faults had a minimal impact on the thermal evolution of the source rocks, they did influence the layers of the hydrocarbon injection into the subsequent local grid refinement model. A total of 113 faults were defined within the Changcheng System–Ordovician, and the data were obtained via interpretation of seismic data provided by the PetroChina Changqing Oilfield Company. According to the tectonic evolution, four periods of fault

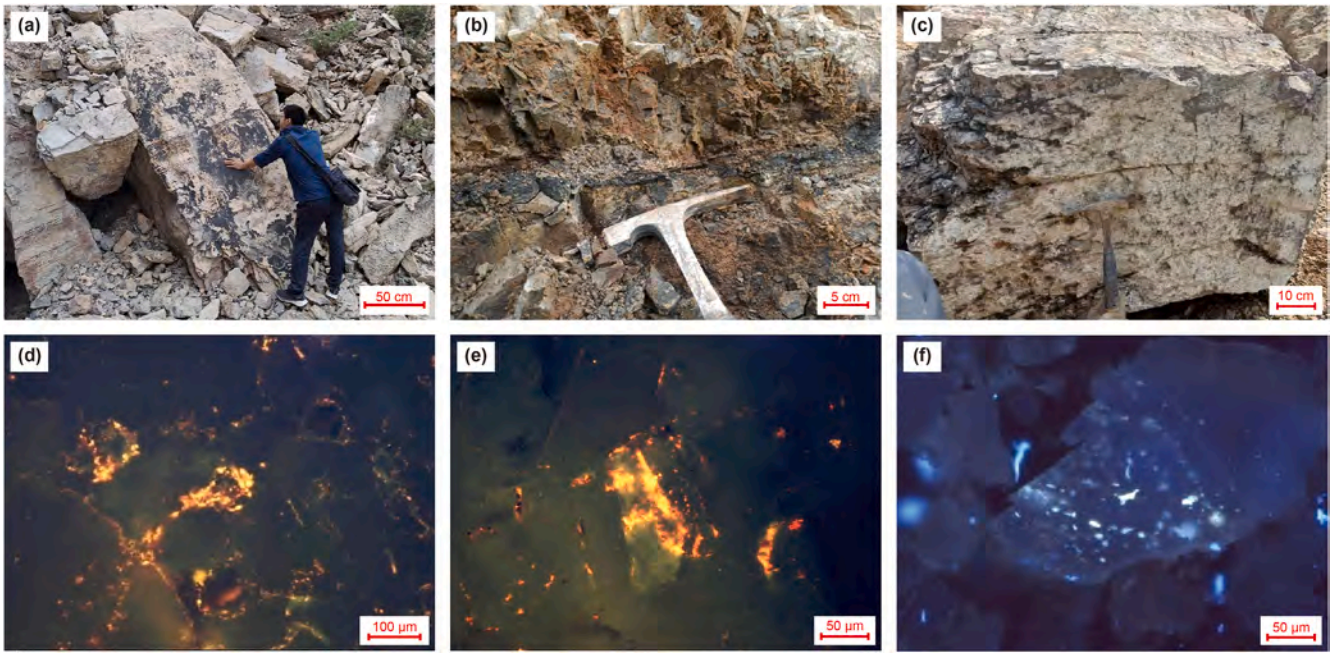

Fig. 12. Bitumen and fluorescence for Mesoproterozoic petroleum system in the Ordos Basin. **(a)** Lamellar distribution of bitumen on the fracture surfaces in a sample from the Qinglong Mountains (Jx); **(b)** zonal distribution of bitumen in a fracture in Tongcheng (Jx); **(c)** bitumen partially filling dolomite solution pores in Tongcheng (Jx); **(d)** orange and brown fluorescence of sandstone from the Zhongtiao Mountains (Ch); **(e)** orange and brown fluorescence of sandstone at 4463.0 m (Ch) in well T59; and **(f)** hydrocarbon fluid inclusions in sandstone at 4958.0 m (Ch) in well GT1. The photomicrographs of the thin sections are courtesy of the PetroChina Changqing Oilfield Company.

Table 3
Saturated hydrocarbon parameters from GC/MS analysis of the chloroform bitumen A in the dolomite, Jixian System, Qinglong Mountains and Tongcheng outcrops.

Sample ID	Pr/nC_{17}	Ph/nC_{18}	Pr/Ph	C_{21}/C_{20}TT	C_{23}/C_{21}TT	Ts/Tm	OEP	Ga/C_{30}H	C_{31}22S/(22R + 22S)	C_{29}20S/(20R + 20S)
QLS-1	0.52	1.01	0.64	2.45	3.06	1.26	0.95	0.17	0.58	0.37
QLS-2	0.47	0.97	0.84	2.14	3.48	1.24	1.00	0.17	0.60	0.24
TC-1	0.50	1.23	0.94	1.88	3.96	1.21	0.93	0.16	0.59	0.35
TC-2	0.46	0.91	0.76	2.33	3.09	1.24	0.92	0.17	0.57	0.34

* Pr/nC_{17} = pristine/*n*-heptadecane; Ph/nC_{18} = phytane/*n*-octadecane; C_{21}/C_{20}TT = C_{21}/C_{20}-13β,14α tricyclic terpane; C_{23}/C_{21}TT = C_{23}/C_{21}-13β,14α tricyclic terpane; Ts/Tm = 18α/17α-C_{27} trisnorneohopane; Ga/C_{30}H = gammacerane/C_{30} hopane; C_{31}22S/(22R + 22S) = 22S/(22R + 22S)-17α,21β-homohopane; and C_{29}20S/(20S + 20R) = 20S/(20S + 20R)-24-ethyl-ααα-cholestane.

activity were defined since the Mesozoic: Late Triassic, Early Jurassic, end Early Cretaceous, and Cenozoic (Yang et al., 2021b, 2024a, 2024b). During these active periods, the shale-to-stratum thickness ratio in each layer approximately characterize the shale gouge ratio (SGR) of the faults within that stratum.

4.2. Input parameters and model validation

The accuracy of the thermal and maturity models depends on the thermal conductivity of the rocks and the boundary conditions. The thermal conductivity and heat production of the rocks were assigned according to the different strata and tectonic elements (Qi, 2018). The boundary conditions include the paleo-water depth (PWD), sediment–water interface temperature (SWIT), and heat flow. In a marine environment, it is generally believed that the PWDs for littoral facies are 0–50 m, for neritic facies are 50–200 m, and for bathyal facies are 200–2000 m. In a continental environment, Yang et al. (2012b) provided a semi-quantitative description of the relationship between the sedimentary facies and PWD in the Triassic sequence based on the fossil assemblages. Consequently, the PWD was estimated using information on the sedimentary facies in each layer. The SWIT was determined using the global mean surface temperature (Wygrala, 1989) in the PetroMod module.

Heat flow plays a critical role in thermal evolution history. The evolution of heat flow in the Ordos Basin since the Mesozoic has been systematically investigated in previous studies (Qi, 2018; Qi et al., 2020; Ren et al., 2020; Yang et al., 2021b, 2024b). However, the pre-Mesozoic heat flow evolution also influenced the thermal evolution of the source rocks in the Changcheng System. The Ordos Basin experienced multi-stage tectonic subsidence before the Mesozoic, which was associated with lithospheric stretching and thinning (Kai et al., 2020). Taking well XT1 as an example, the McKenzie model (1978) was used to reconstruct the evolution of heat flow before the Mesozoic. Fig. 14(a)–(c) presents the simulation results of the burial and thermal history, as well as maturity model calibration for well XT1, showing good correlations between the measured and simulated vitrinite reflectance values. Since the Proterozoic, the strata in this well have experienced four heat flow peaks: (1) the Changcheng (61.3 mW/m^2), (2) Middle Cambrian–Ordovician (60.5 mW/m^2), (3) Early–Middle Triassic (59.5 mW/m^2), and (4) Early Cretaceous (86.4 mW/m^2). Under this heat flow evolution scenario, the top of the Changcheng System entered the early oil window in the Late Ordovician, and then, the oil–gas generation was hindered by uplift and erosion, leading to a transformation ratio (TR) of the source rocks of less than 12%. With the rapid subsidence during the Triassic, the top of the Changcheng System transitioned into the gas-generation

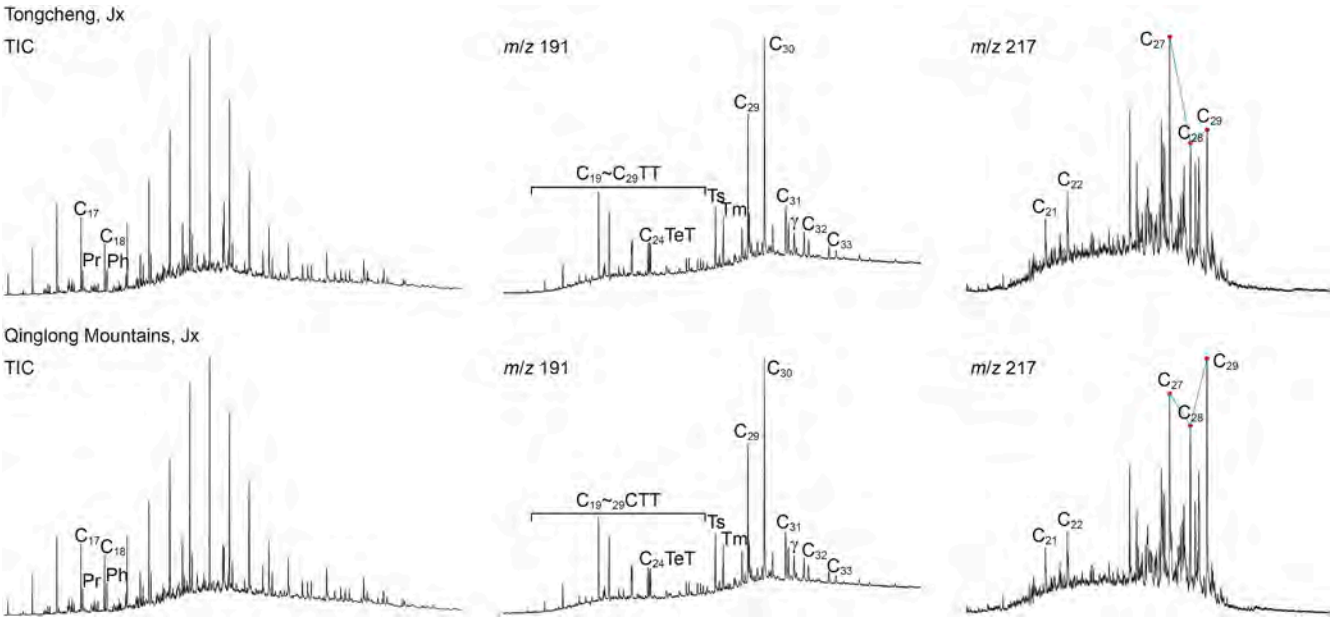

Fig. 13. Mass chromatograms showing the distribution of the *n*-alkanes (TIC), hopanes (*m/z* 191), and steranes (*m/z* 217) in the chloroform bitumen A extracted from dolomite in the Jixian System of the Qinglong Mountains and Tongcheng outcrops.

stage, resulting in a rapid increase in the TR of the source rocks. Finally, in the Early Cretaceous, the vitrinite reflectance reached its peak and the rocks entered an overmature stage.

Using the above-described method, simulations were conducted to reconstruct the pre-Mesozoic heat flow evolution by analyzing the burial and thermal histories of 45 wells. The measured borehole temperatures and vitrinite reflectance calibration of partial wells are shown in Fig. 14(d)–(g). Although there may be some uncertainty in the simulation results of the heat flow evolution before the Mesozoic, stemming from differences in the ancient and modern lithosphere thicknesses and the applicability of the McKenzie model to the Mesoproterozoic rift trough, they nonetheless illustrate the disparities between the rapid subsidence and slow subsidence stages, and can be used to reconstruct the thermal and maturity evolution from the Proterozoic to the present with relatively good accuracy.

4.3. Local grid refinement

The 3-D hydrocarbon migration simulation provides more precise constraints on the petroleum movement, entrapment, and leakage (Duran et al., 2013) and is central to the analysis and evaluation of petroleum systems. The PetroMod software was used to simulate the thermal evolution of the source rocks in the Changcheng System by applying the Easy%R_o model at the basin scale. Furthermore, the flow paths and fluid potential beneath the Cambrian regional caprocks were analyzed to delineate the two major migration and accumulation systems: the Dingbian–Wushenqi (Ding–Wu) system and the Huanxian–Yan'an (Huan–Yan) system (Fig. 15(a)). This division was based on the merging and splitting of migration and accumulation units during the evolution. Due to the absence of Lower Paleozoic regional caprocks in both the southern and northern parts of the Mesoproterozoic petroleum system, lithological assignments were carried out for the Changcheng–Ordovician reservoir–caprock assemblages of these two systems, with a grid spatial resolution of 1 km × 1 km. These assemblages include four types of reservoir rocks in the Changcheng System, weathering crust and dolomite reservoir rocks in the Middle and Upper Cambian–Ordovician strata, marine shale and tight carbonates within the transgressive systems tract in the Cambrian strata, and marine shale and evaporites in the Ordovician strata (data from the PetroChina Changqing Oilfield Company). The correspondence between the layers in both the parent model and the child model (high resolution) was defined. Additional grid cells were inserted into the parent model near the interfaces between the parent and child models, along with additional coupling conditions, to accurately determine the hydrocarbon injection positions and fluxes generated from the parent model. Finally, a nested simulation with local grid refinement was conducted to analyze the characteristics of hydrocarbon migration and accumulation using the invasion percolation method.

Local grid refinement allows for a more accurate representation of the underground lithology, structure, and other geological characteristics, and the simulation results are also closer to the actual geology. First, the difference in the meshing results at different resolutions was compared using plan-view and cross-sectional analysis. As shown in Fig. 15(b), the meshing results at the basin scale (10 km × 10 km) clearly depict the west-dipping monoclinal structure of the top surface of the Cambrian strata. After conducting local grid refinement (1 km × 1 km) of the Huan–Yan system, numerous structural details were identified on this surface, such as several low-amplitude structures with closure heights of 40–80 m in the NT1–LA1–QT1 wellblocks (Fig. 15(c)). It was also found that the anticlinal core identified by the local grid refinement did not align with that of the basin-scale grid, based on the correlation results of the Cambrian stratigraphic profiles, as exemplified by a deviation of approximately 1.5 km in the YT1 wellblock, as well as by discrepancies in the meshing results pertaining to the lithological distribution (Fig. 15(d)). Furthermore, the addition of additional grids into the parent model, along with the introduction of additional coupling conditions, significantly influenced the simulation results. As shown in Fig. 15(f), during the simple nested simulation, hydrocarbons were not introduced into the child model at the grid cells corresponding to the Huating area, and no hydrocarbon accumulation in the Zhangxia Fm. was observed in the eastern part of Huating at 206 Ma. After adding additional grids into the parent model and introducing the additional coupling conditions, the grid cells in the Huating area were found to contain conduit system facies. These facies were

Table 4
Input parameters used for the 3-D basin modeling of the petroleum system.

Simulation stage	Stratigraphy			Ages from, Ma	Ages to, Ma
	System	Fm./Mbr.	Code		
1	Quaternary		Q	2.6	0.0
2	Cretaceous	Erosion	Ero.	96.0	2.6
3		Yijun–Luohe	K	145.0	96.0
4	Jurassic	Erosion	Ero.	161.0	145.0
5		Anding	J_2	167.0	161.0
6		Erosion	Ero.	169.0	167.0
7		Fuxian–Zhiluo	J_{1-2}	183.0	169.0
8	Triassic	Erosion	Ero.	206.0	183.0
9		Yanchang	T_3y	227.0	206.0
10		Liujiagou–Zhifang	T_{1-2}	251.0	227.0
11	Permian	Shiqianfeng	P_3q	257.0	251.0
12		Upper Shihezi	P_2h^2	272.0	257.0
13		Lower Shihezi	P_2h^1	280.0	272.0
14		Shanxi	P_1s	290.0	280.0
15		Taiyuan	P_1t	296.0	290.0
16	Carboniferous	Benxi	C_2b	311.0	296.0
17	Ordovician	Erosion	Ero.	450.0	311.0
18		Pingliang–Beiguoshan	O_3	458.0	450.0
19		6th member of Majiagou Fm.	O_2m^6	463.0	458.0
20		5th member of Majiagou Fm.	O_2m^5	468.0	463.0
21		4th member of Majiagou Fm.	O_2m^4	470.0	468.0
22		3rd member of Majiagou Fm.	O_1m^3	473.0	470.0
23		2nd member of Majiagou Fm.	O_1m^2	475.0	473.0
24		1st member of Majiagou Fm.	O_1m^1	477.0	475.0
25		Liangjiashan	O_1l	481.0	477.0
26		Yeli	O_1y	485.0	481.0
27	Cambrian	Erosion	Ero.	490.0	485.0
28		Sanshanzi	$\in_3s$	500.0	490.0
29		Zhangxia	$\in_2z$	510.0	500.0
30		Mantou	$\in_2m$	518.0	510.0
31		Zhushadong	$\in_1z$	520.0	518.0
32		Xinji	$\in_1x$	521.0	520.0
33	Sinian	Luoquan	Z	541.0	521.0
34	Jixian	Erosion	Ero.	1400.0	541.0
35		Jixian	Jx	1600.0	1400.0
36	Changcheng	Changcheng	Ch	1800.0	1600.0

connected to the source rocks of the Changcheng System in the parent model via faults, allowing hydrocarbon injection into the child model in this region and resulting in hydrocarbon migration and accumulation in the eastern part of Huating. All of these factors may affect the simulation results of the hydrocarbon migration and accumulation. Finally, the simulation results with and without local grid refinement were compared. From the perspective of the hydrocarbon migration simulation at the basin scale, there were two major migration and accumulation systems in the Mesoproterozoic petroleum system, and the hydrocarbon accumulation in the basin-scale simulation basically appeared in the nested simulation of local grid refinement. However, the nested simulation results provide more detailed information, such as the hydrocarbon accumulation in the Changcheng System in the E6–T93–T59 wellblocks. It is important to note that the nested simulation results reveal that the oil–gas accumulation was not evident in the basin-scale simulation, such as the hydrocarbon accumulation in the Cambrian strata in the L73–NT1–HT2 wellblocks (Fig. 15(e)). This discrepancy can be attributed to the local grid refinement, which identified several low-amplitude structures on the west-dipping monoclinal structure. In conclusion, taking into account the efficiency and accuracy of the numerical simulation, the nested simulation not only significantly reduced the simulation time but also yielded results that are more consistent with the fluorescence data for wells T59 and GT1, as well as the bitumen data for the Zhongtiao Mountains and Tongcheng.

5. Modeling results and discussion

5.1. Thermal maturity evolution of source rocks

The thermal maturity of source rocks in the Changcheng System was reconstructed through numerical simulation. As shown in Fig. 16, at the end of the Cambrian (485 Ma), source rocks in the central and western parts of the N–M Rift and DB rift had begun to mature, as had those in the southwestern part of the J–S Rift. Subsequently, the basin experienced extensive carbonate deposition during the Ordovician, followed by tectonic erosion associated with the Caledonian event. During the Late Carboniferous (311 Ma), the maturity of source rocks had significantly increased compared to the Late Cambrian, with those in the western parts of the N–M Rift and DB rift, as well as the southern part of the J–S Rift, reaching the wet gas stage. During the Late Permian (251 Ma), the maturity distribution pattern remained largely consistent with that of the Late Carboniferous, albeit showing a slight increase. For instance, source rocks in the Yinchuan–Guyuan area had entered the dry gas stage. During the Late Triassic (206 Ma), under the influence of thick Triassic deposits, all source rocks within the Changcheng System had begun to mature, with the central part of the WBU and nearly the entire WMTB entering the wet gas–dry gas transition stage. During the Late Jurassic (161 Ma), the western portions of the N–M Rift and DB rift had reached the overmature stage, whereas the central and eastern regions of both rifts were predominantly in the wet gas–dry gas stage. In the J–S Rift, the central and western areas were in the wet gas–dry gas stage, while certain zones in the eastern part remained in the main oil–late oil stage. At present (~0 Ma), all source rocks have entered the dry gas to overmature stage, primarily due to thick sedimentary deposits and a heat flow peak during the Early Cretaceous. Specifically, the southern portion of the WBU and nearly the entire WMTB have reached the overmature stage, while the remaining areas remain in the dry gas stage.

5.2. Hydrocarbon accumulation events

There are two sets of potential source rocks in the Mesoproterozoic petroleum system in the Ordos Basin. One set consists of the source rocks of the Baicaoping Fm., which are primarily developed in semi-deep marine facies in the western and northern parts of the basin. The other set consists of the source rocks of the Cuizhuang Fm., which are primarily distributed in semi-deep marine facies in the southern part of the basin. The source rocks are dominated by type I kerogen, with TOC contents of >2.0% and ~0.6% in the deep rift region and in the margin rift region, respectively. In addition to the quartz sandstone in the littoral–neritic facies in the Changcheng System, there are weathering crust and dolomite reservoir rocks in the Middle and Upper Cambian–Ordovician strata, as well as reef-bank body reservoir rocks in an L-shaped platform-margin zone in the Ordovician strata (Guo et al., 2014; Du et al., 2019; Zhou et al., 2023). The period of trap formation was primarily associated with the peripheral foreland basin stage in the Middle–Late Mesozoic.

According to the analysis of fluid inclusions, there were three critical periods for hydrocarbon accumulation in the Lower Paleozoic oil–gas reservoirs, including the Middle and Late Jurassic, the Early Cretaceous, and a readjustment period since the Late Cretaceous (Guo et al., 2014; Chen et al., 2023). However, it should be noted that all the source rocks in the Changcheng

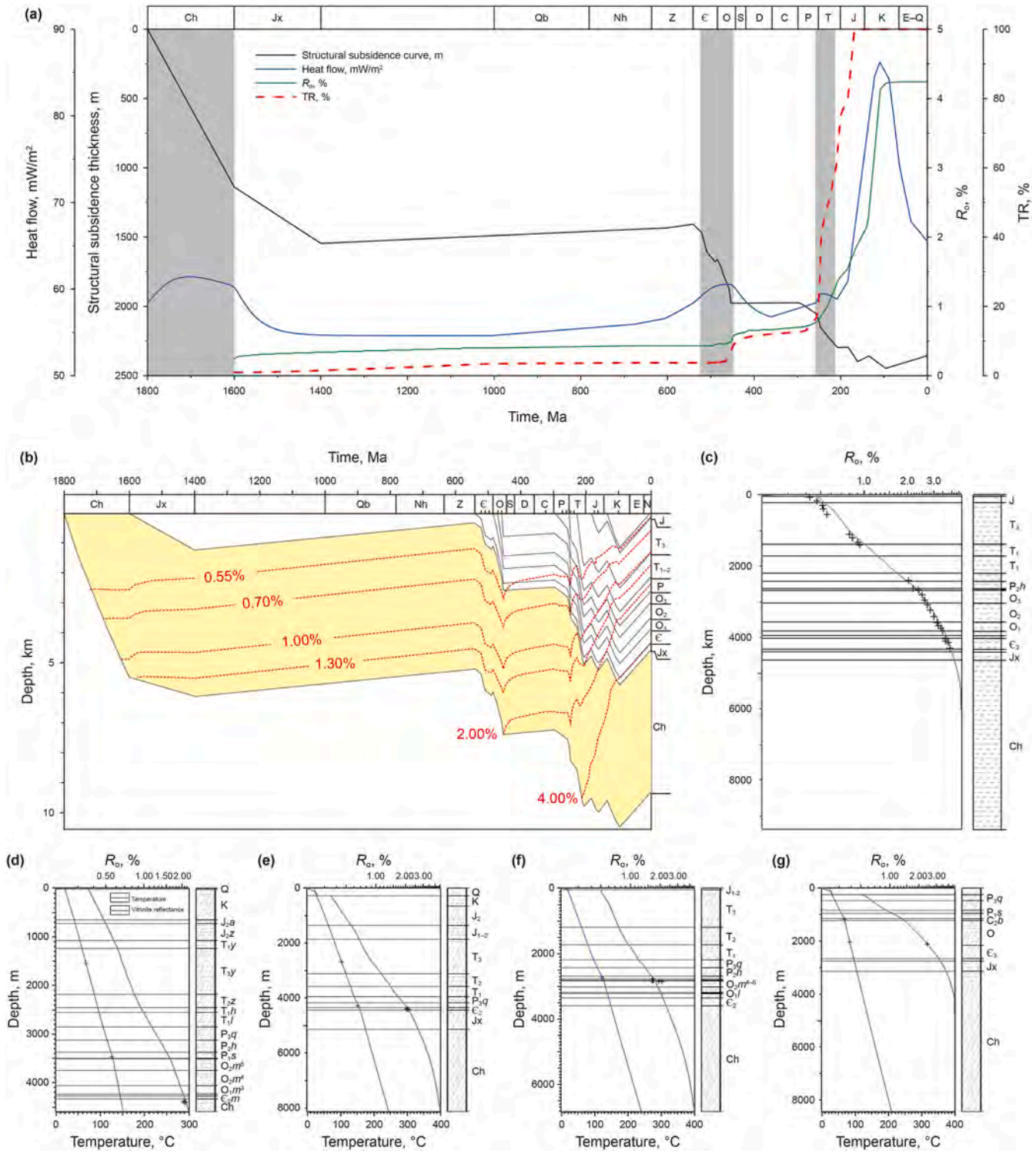

Fig. 14. **(a)** Map showing the evolution of the subsidence curve, vitrinite reflectance R_o, transformation ratio TR, and heat flow, **(b)** burial-thermal evolution, **(c)** maturation model calibration for well XT1, **(d)** temperature maturation model calibration for well T59, **(e)** temperature maturation model calibration for well L27, **(f)** temperature maturation model calibration for well Y63, and **(g)** temperature maturation model calibration for well R3.

System had begun to mature, and the Cambrian seal rocks had acquired the ability to seal natural gas since the Late Triassic, indicating that this period was at least a critical period for the Mesoproterozoic petroleum system. When integrated with the results for the hydrocarbon generation and expulsion, as well as the characteristics of hydrocarbon accumulation in the Lower Paleozoic, the critical periods for the Mesoproterozoic petroleum system can be classified into four periods: T_2–T_3, J_2–J_3, K_1, and N–Q, respectively (Fig. 17). Destruction and reworking of the early-formed hydrocarbon reservoirs were commonplace, particularly during the uplift stages. Since the Late Cretaceous, the basin has experienced significant uplift and erosion, representing a period of both readjustment and preservation of the oil–gas reservoirs.

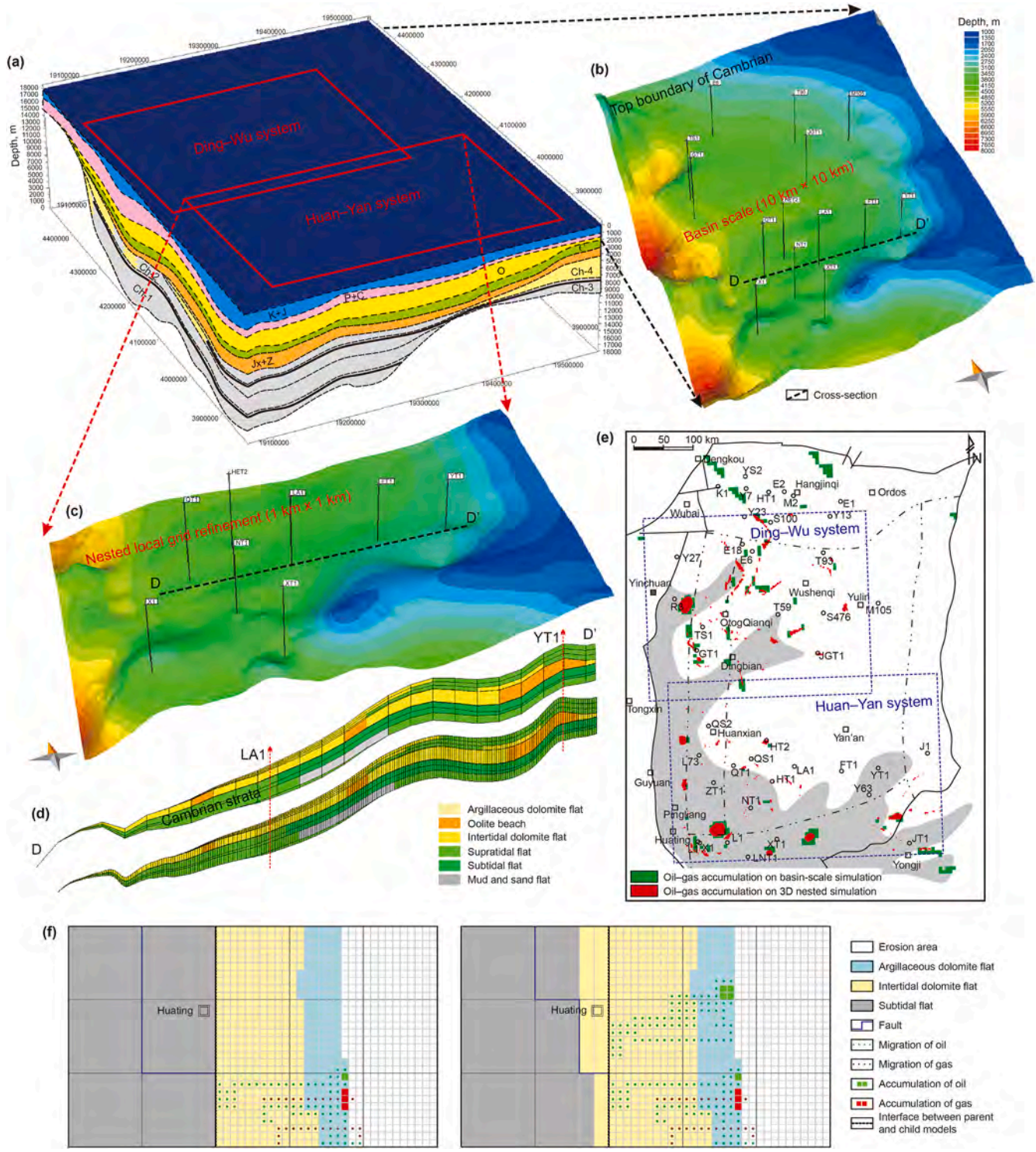

Fig. 15. **(a)** Map showing the 3-D conceptual geologic model (at present) of the Mesoproterozoic petroleum system in the Ordos Basin, with Ch-1 to Ch-4 referring to the Baicaoping, Beidajian, Cuizhuang, and Luoyukou formations of Changcheng System, respectively, **(b)** the burial depth of the top boundary of the Cambrian strata at the basin scale, **(c)** the burial depth of the top boundary of the Cambrian strata in the Huan–Yan system after local grid refinement, **(d)** comparison of the meshing results for the Cambrian lithologic cross-section (see (b) for location) at the basin scale and the migration and accumulation system scale, **(e)** comparison of the simulation results at the basin scale and the nested migration and accumulation system scale, and **(f)** comparison of the simulation results before and after inserting additional grid cells into the parent model and introducing additional coupling conditions.

5.3. Plan view of petroleum system

The accuracy of simulation results is crucial for basin modeling. However, the sporadic Meso–Neoproterozoic bitumen shows and the fluorescence observed in the Ordos Basin introduce challenges in verifying the accuracy of the hydrocarbon migration simulation results. Therefore, it is essential to consider all potential evidence as comprehensively and systematically as possible. From the simulation results, it is evident that within the Proterozoic strata, minor oil–gas accumulations were identified in wells T59 and GT1

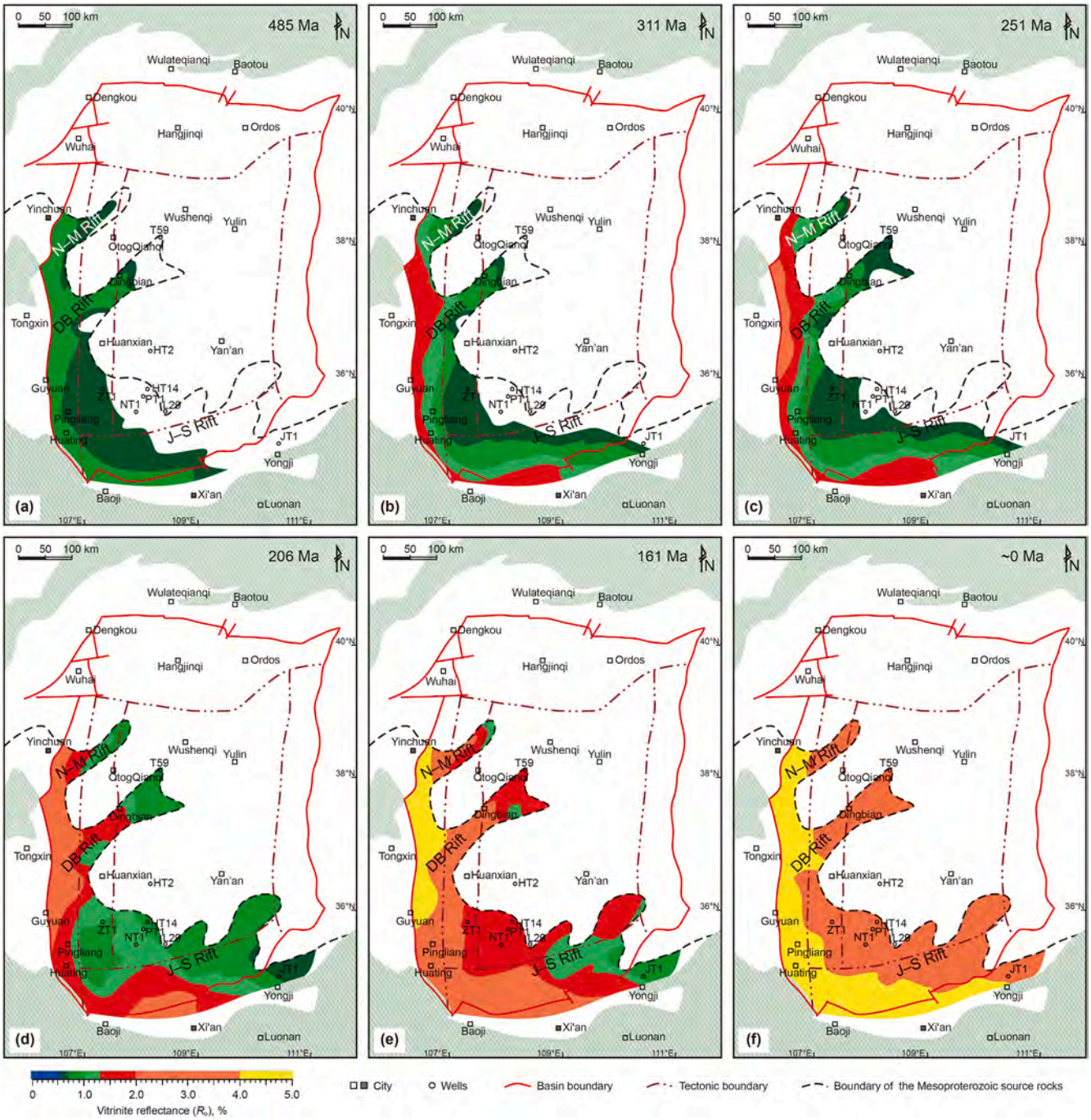

Fig. 16. Maturity maps of the source rocks for the Changcheng System in the Ordos Basin. **(a)** Late Cambrian, **(b)** Late Carboniferous, **(c)** Late Permian, **(d)** Late Triassic, **(e)** Late Jurassic, and **(f)** the present.

during the Late Triassic, a small oil–gas accumulation was observed in the Tongcheng region during the Late Jurassic, and a significant natural gas accumulation is currently present in well JGT1. Meanwhile, a series of small-scale oil–gas accumulations simulated in the QT1–ZT1–NT1–HT1 wellblocks within the Cambrian strata are consistent with the current exploration situation of this region. That is, low production gas reservoirs are developed in many wells located at the top of the Cambrian weathering crust in this region, and the Changcheng System is considered a potential source rock (Wu et al., 2024b; Huang et al., 2025). However, we were unable to successfully simulate the oil–gas accumulation near Qinglong Mt. Due to the tight reservoir rock in this outcrop, no paleo-reservoir was formed, as solid bitumen filled several fractures in vein-like shapes. Because the basin modeling has limitations in detailing the local development of fractures, it may not fully capture certain geological complexities. Nevertheless, despite the lack of simulated hydrocarbon accumulation in Qinglong Mt., the simulation results remain generally reliable.

The simulation results indicate that the source rocks in the Ding–Wu system underwent widespread maturation during the Late Triassic. The R_o values of the source rocks in the N–M Rift and DB Rift within the WMTB reached 2.0%, and they entered the dry gas stage. The R_o values of the source rocks in the THD and YSS

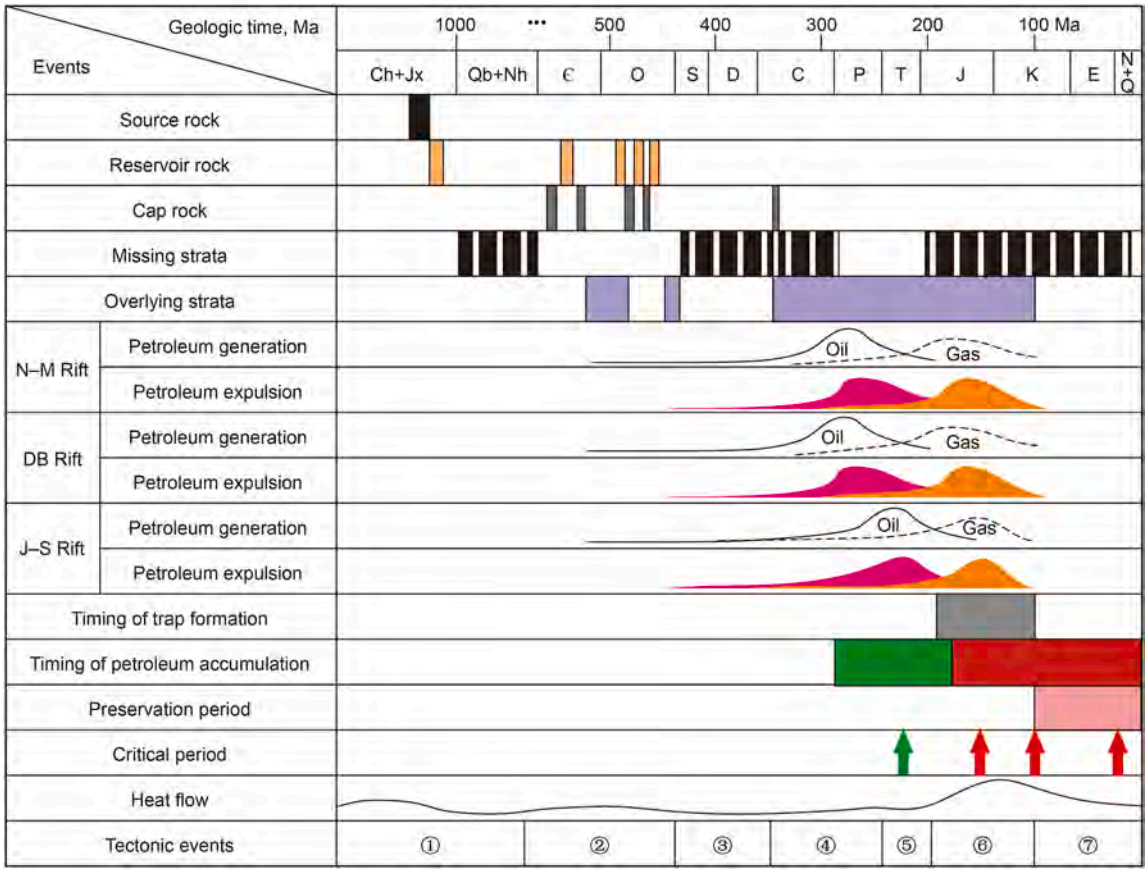

Fig. 17. Chart presenting the events related to the Mesoproterozoic petroleum system, including hydrocarbon generation, migration, and accumulation in the Ordos Basin during the (1) rift basin stage, (2) passive margin basin stage, (3) collisional orogeny stage, (4) peripheral rifting stage, (5) depression basin stage, (6) peripheral foreland basin stage, and (7) peripheral faulted-depression stage.

were all >0.7%, and they entered the main oil–wet gas stage. During this period, large-scale oil–gas accumulation occurred in the southern and northern parts of OtogQianqi, primarily within the Changcheng System and Ordovician strata, and both the well GT1 and well T59 exhibited a small amount of oil–gas accumulation in the Changcheng System. During the Late Jurassic, the western parts of the N–M and DB rifts reached an overmature stage, with R_o values of >4.0%, while the central and eastern sections of these two rifts were primarily in the wet gas–dry gas stage and had entered a peak period of gas generation, indicating that this was a critical period for gas accumulation. The hydrocarbon primarily accumulated in the Changcheng System and Cambrian–Ordovician strata in the Central Paleohigh, the Ordovician structural highs on the western side of the Central Paleohigh, and the Changcheng System facies change and unconformity-related traps on the eastern side of the Central Paleohigh. During the Early Cretaceous, the source rocks in the WMTB were in the overmature stage, while in the other regions, the source rocks were in a dry gas stage. The oil–gas distribution during this period was somewhat similar to that in the Late Jurassic. However, due to the continuous gas generation of the source rocks on both the north and south sides of OtogQianqi, there was a significant increase in the hydrocarbon accumulation in the OtogQianqi area. Additionally, the uplift and erosion events in the Late Jurassic led to a northeastward shift (into the Ordovician strata) in the hydrocarbon accumulation within the Changcheng System in the T59–T93 wellblocks. Since the Late Cretaceous, there has been a readjustment period for the oil–gas reservoirs, during which the oil and gas in the OtogQianqi area was readjusted toward the eastern and northern Ordovician and Changcheng System on a large scale (Fig. 18).

From a single stratum perspective, within the Ding–Wu system, the Proterozoic oil–gas accumulations were primarily located within the Changcheng System. These accumulations were mainly trapped in the paleohigh during the Late Triassic and then gradually shifted towards the northeast and were re-formed after the Jurassic. The Cambrian oil–gas accumulations were relatively undeveloped and was primarily located in the paleohigh and structural highs on its western flank. The Ordovician hydrocarbon accumulations were primarily distributed in the paleohigh and the structural highs on its western flank during the Late Triassic–Early Cretaceous. Subsequently, since the Late Cretaceous, they have shifted significantly and extensively towards the northeast.

The Huan–Yan system was characterized by the development of numerous faults that were connected to the source rocks, and the hydrocarbon primarily accumulated in the Cambrian–Ordovician strata. The R_o values of the source rocks in the J–S Rift exceeded 1.3% in the western part of the WMTB and the southern part of the WBU during the Late Triassic, indicating that they had entered the wet gas stage. In addition, the R_o values of most of the source rocks were within 0.7%–1.3%, suggesting that this was the main oil to late oil stage. During this period, the oil and gas primarily accumulated within the Cambrian–Ordovician strata in the Central Paleohigh, as well as within the Cambrian–Ordovician strata on the western and southern sides of the Central Paleohigh, particularly within the Ordovician strata. During the Late Jurassic, the southwestern part of the J–S Rift was in a stage characterized by dry gas, while some areas in the eastern part of the J–S Rift were still in the main oil to

late oil stage. During this period, the Tongcheng region experienced a small amount of oil–gas accumulation in the Proterozoic strata. During the Early Cretaceous, the R_o values of the source rocks in the WMTB and the southwest part of the WBU exceeded 4.0%, indicating that they were in the overmature stage, while those in other areas transitioned into the dry gas stage. In the Late Jurassic–Early Cretaceous, the source rocks experienced a peak period of gas generation, and the oil–gas accumulation in the Cambrian strata increased significantly within the range of the paleohigh, while the hydrocarbon accumulation in the Ordovician strata on the western and southern sides of the paleohigh remained relatively unchanged. Since the Late Cretaceous, the Ordovician hydrocarbon accumulation in the eastern part of the paleohigh has leaked upward, while the hydrocarbon accumulation in the Cambrian strata shifted towards the northeastern region along the unconformity at the top of the Cambrian strata and then re-formed (Fig. 18). The large number of mud logging oil–gas shows in the Cambrian weathering crust in the southwestern part of the basin may be related to the Mesoproterozoic petroleum system.

From a single stratum perspective, within the Huan–Yan system, the oil–gas accumulation in the Proterozoic strata primarily occurred within the Changcheng System, and large-scale accumulation was distributed in the area to the north of well JT1, which has been influenced by the readjustment period since the Late Cretaceous. The oil–gas accumulation in the Cambrian strata was distributed within the range of the paleohigh. The southwestern oil–gas accumulation was controlled by the major accumulation period in the Triassic–Early Cretaceous, and the northeastern oil–gas accumulation was influenced by the readjustment period since the Late Cretaceous. The oil–gas accumulation in the Ordovician strata was mainly distributed in the southern part of the paleohigh, which was controlled by the major accumulation period in the Triassic–Early Cretaceous.

According to the plan view of the multiple critical periods, the hydrocarbon migration and accumulation in the Mesoproterozoic petroleum system was primarily influenced by the major accumulation period in the Triassic–Early Cretaceous and the readjustment period since the Late Cretaceous. The oil–gas reservoirs formed in the major accumulation period were mainly distributed within the Central Paleohigh and its adjacent areas. During the readjustment period, oil and gas readjustment and reaccumulation occurred along the unconformity towards the northeast region on a large scale, and that in the Dingbian–Yulin area was the most significant.

5.4. Profile of petroleum system

Two-dimensional (2-D) geological profiles provide a more accurate reflection of stratigraphic, lithological, and structural characteristics, making them a valuable complement to 3-D simulations. The calculation process of a 2-D simulation involves meshing geological profiles, which requires that the same stratum can only occur once in a vertical grid. This presents a challenge for 2-D geological modeling when dealing with repeated strata or thrust systems. To address this issue, the PetroMod software has introduced the Block module for complex geological modeling, such as modeling foreland basins (Hantschel and Kauerauf, 2009). The function of the Block module is to divide the geological model containing repeated strata into blocks using faults or strata as boundaries and to carry out block meshing so as to ensure that each block unit does not contain repeated strata. In addition to eliminating the issue of repeated strata, the Block module accurately describes the fault morphology and structural and stratigraphic characteristics of nearby faults.

In this study, an east–west balanced cross-section in the southern Ordos Basin was selected for hydrocarbon migration simulation. On the basis of the block division and meshing, a geological model was constructed based on drilling data, logging data, and sedimentary facies data. Finally, the hydrocarbon migration was simulated using the invasion percolation method, and profiles for multiple critical periods were generated.

The western part of profile AB contains two sets of potential source rocks, namely, the Baicaoping Fm. and Cuizhuang Fm. The simulation results indicate that the source rocks began to mature on a large scale during the Permian, but this did not result in the formation of significant hydrocarbon accumulations. During the Late Triassic, the source rocks were in a wet gas stage, and a certain scale of oil–gas accumulation occurred within the Cambrian and Ordovician strata in the palaeohigh, as well as oil–gas accumulation within the Changcheng System, below the source rocks in the thrust belt. At this time, due to fault activity, oil and gas also accumulated within the shallow Permian strata. During the Late Jurassic, most of the source rocks entered a dry gas stage and experienced a peak period of gas generation, resulting in a significant increase in oil–gas accumulation within the Changcheng System below the source rocks in the Cuizhuang Fm., as well as hydrocarbon accumulation within the Cambrian and Ordovician strata. The source rocks buried below 8.5 km reached an overmature stage during the Early Cretaceous, and the source rocks above also basically entered a dry gas stage. The oil–gas accumulation during this period was largely consistent with that during the Late Jurassic. Along with uplift and erosion since the Late Cretaceous, the oil–gas reservoirs in the paleohigh have shifted towards the eastern part of the basin and reaccumulated, and there are gas layers in the Cambrian strata in wells ZT2, L2, and L9, which is consistent with the current hydrocarbon shows (Fig. 19).

The profiles for the multiple critical periods indicate that the hydrocarbon reservoirs were primarily developed within the Cambrian–Ordovician strata in the paleohigh, Changcheng System on the western side of the paleohigh, as well as in the shallow Permian strata as a result of fault activity during the major accumulation period in the Triassic–Early Cretaceous. Since the Late Cretaceous, the hydrocarbon reservoirs have shifted eastwards along the unconformities of the Cambrian and Ordovician.

5.5. Preferential petroleum accumulation sites

In view of the complex simulation results regarding multi-kitchen and multi-stage hydrocarbon generation, migration, and accumulation, as well as multi-stage readjustment and reaccumulation within the Mesoproterozoic petroleum system, the distribution of flow paths within the migration and accumulation unit was characterized based on hydrocarbon accumulation dynamics at the scale of migration and accumulation unit (system). Furthermore, the factors influencing the simulation results and the preferential accumulation sites were analyzed in each period at the migration and accumulation unit scale by tracing the dynamic processes of each hydrocarbon accumulation pool, combined with the source rock thermal evolution, tectonic evolution, and hydrocarbon migration pathways.

Taking the Ding–Wu system as an example, we provide a brief explanation of the hydrocarbon accumulation process in the OtogQianqi migration and accumulation unit in the Changcheng System (Fig. 20). During the Late Triassic, the OtogQianqi–Yanchi region was located in the high structural position, and the Changcheng System source rocks began to mature fully. Due to fault activity, this period was the first large-scale oil–gas accumulation period. According to the fluid

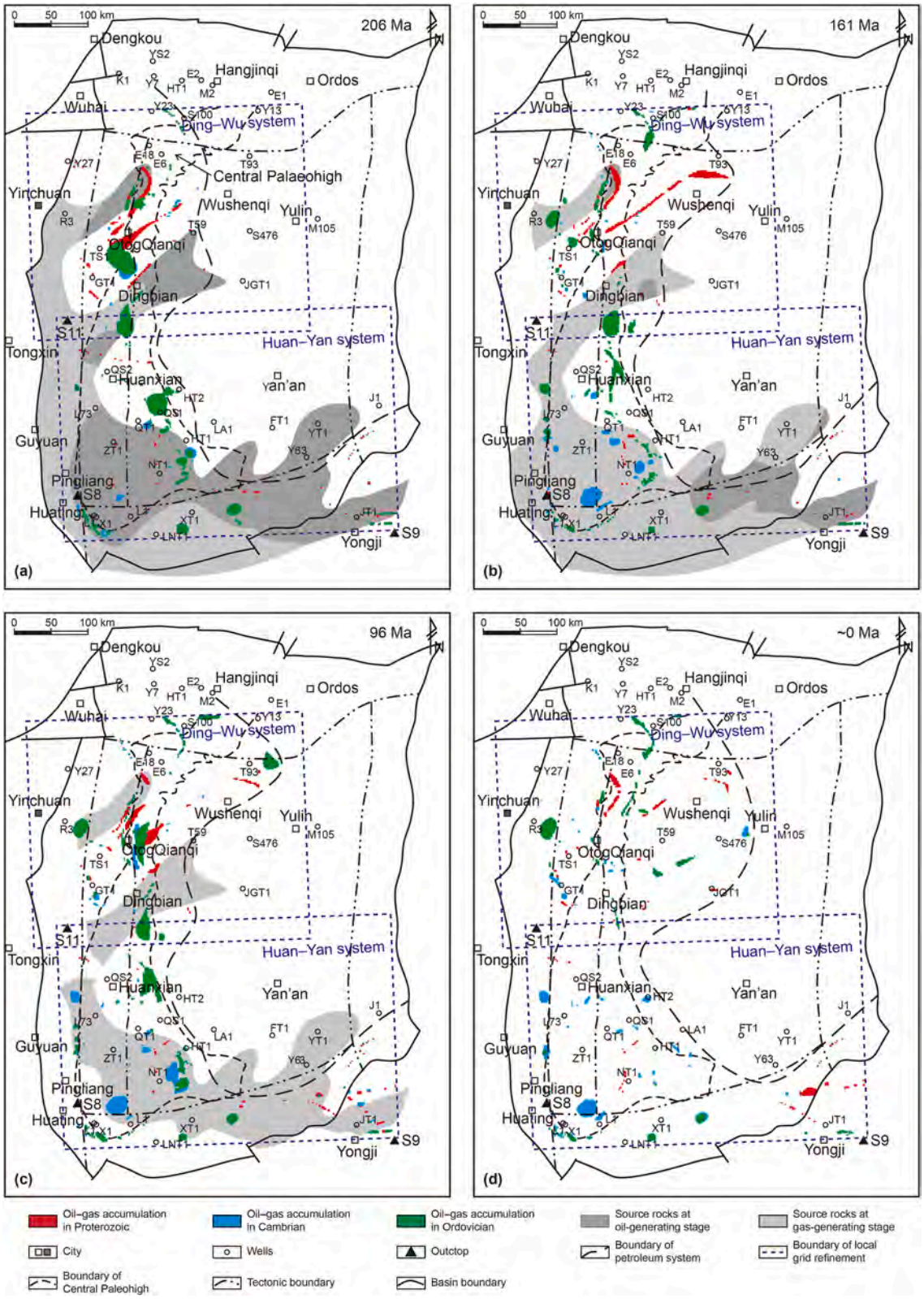

Fig. 18. Plan views of multiple critical periods for the Mesoproterozoic petroleum system in the Ordos Basin. **(a)** Late Triassic, **(b)** Late Jurassic, **(c)** late Early Cretaceous, and **(d)** the present.

potential characteristics under the regional Cambrian caprocks, the Mesoproterozoic strata can be divided into five units. In the OtogQianqi unit, a series of oil–gas accumulation zones formed in the structural highs and unconformity-related traps within the Beidajian Fm. due to the hydrocarbon supply from the double rifts. For example, the fluorescence in well GT1 confirms the occurrence of hydrocarbon migration during this period. During the Late Jurassic, the Ordos Basin was a peripheral

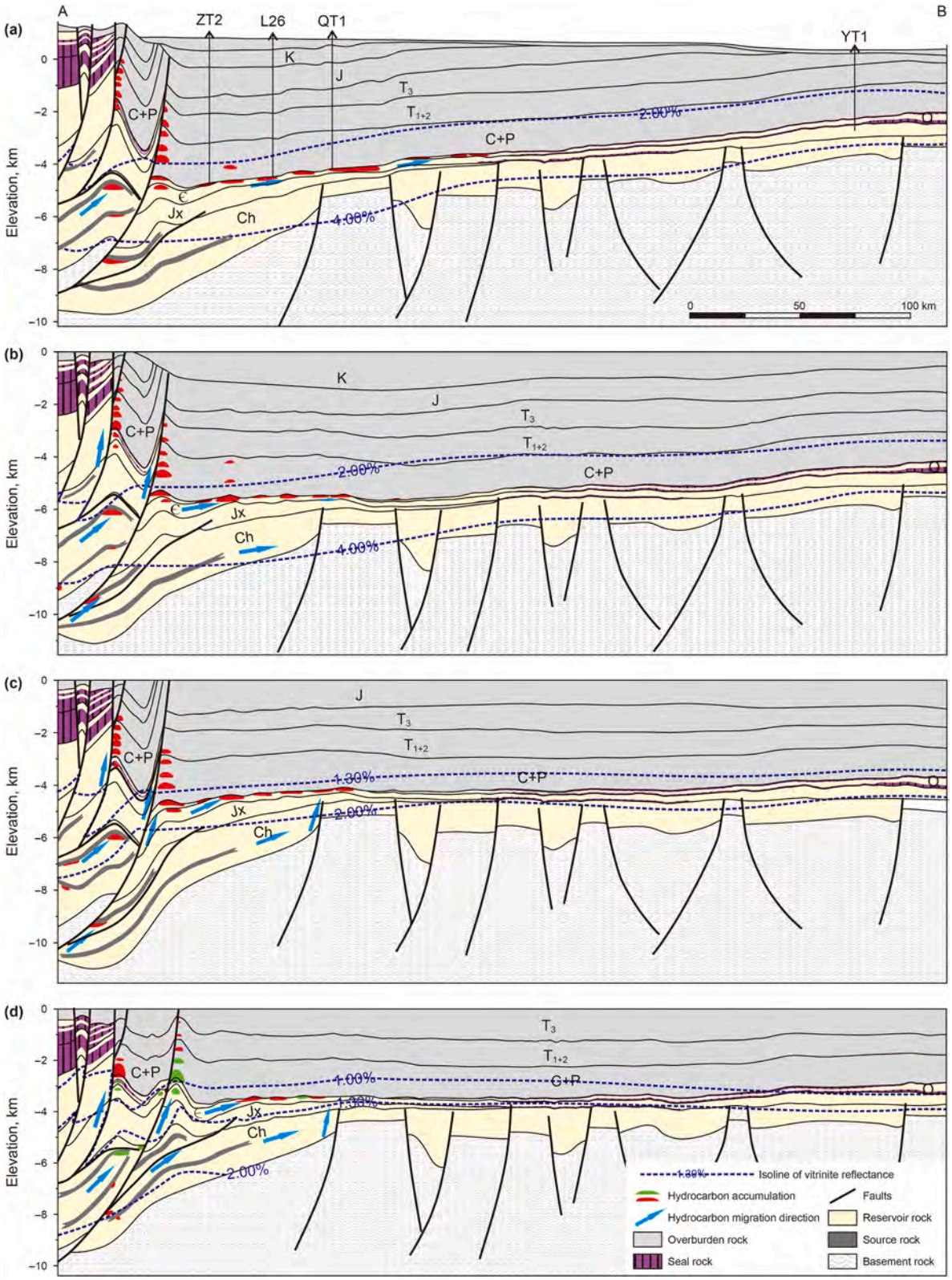

Fig. 19. Profiles showing multiple critical periods for the Mesoproterozoic petroleum system in the Ordos Basin: **(a)** the present, **(b)** late Early Cretaceous, **(c)** Late Jurassic, and **(d)** Late Triassic. The location of the profile AB is shown in Fig. 3.

foreland basin, and significant faulting activity occurred. The high structural position shifted towards the OtogQianqi region. The source rocks entered a peak period of gas generation during this period, and this was the second large-scale oil–gas accumulation period. As a result of the destruction and readjustment of the early formed oil–gas reservoirs, as well as the hydrocarbon supply from the double rifts, the oil and gas migrated and accumulated in the OtogQianqi region.

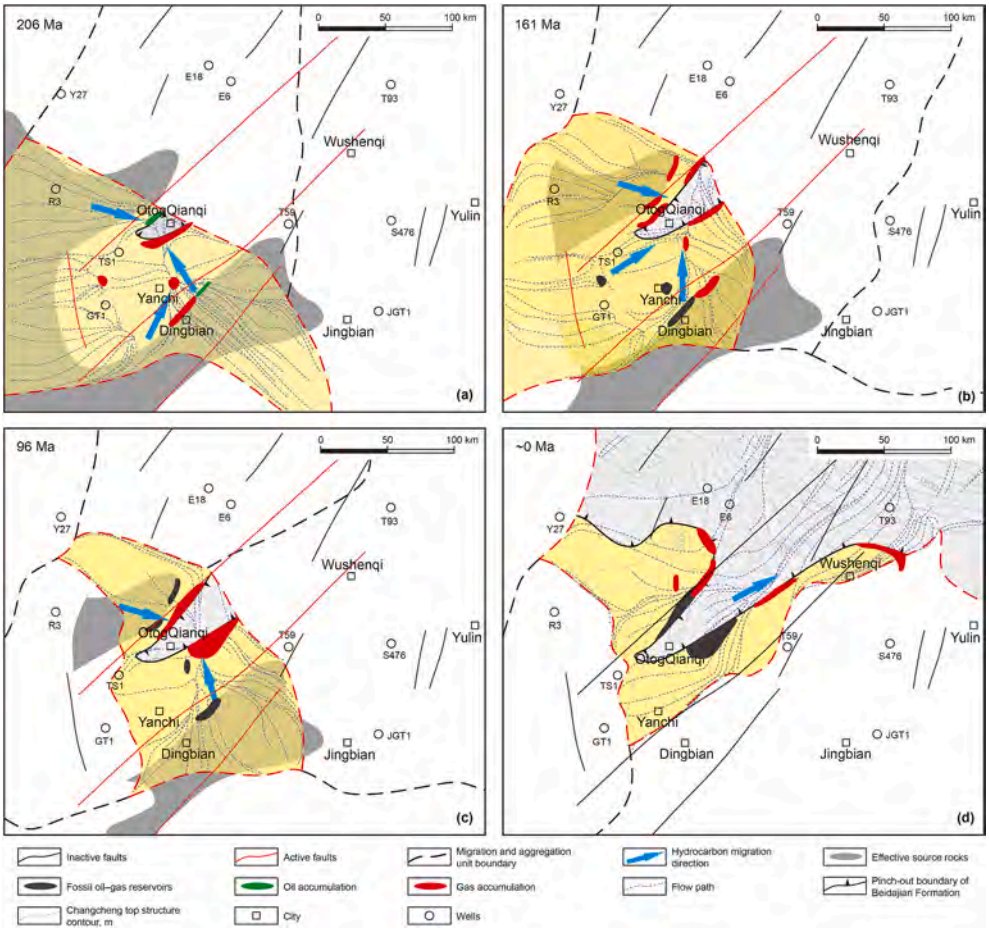

Fig. 20. Map showing the migration and accumulation units, flow lines, and hydrocarbon migration and accumulation processes in different periods for the Changcheng System in Ordos Basin. **(a)** Late Triassic, **(b)** Late Jurassic, **(c)** late Early Cretaceous, and **(d)** the present.

During the Early Cretaceous, the basin reached its maximum burial depth. This was the third large-scale oil–gas accumulation period. The distribution characteristics of the units under the regional caprocks were notably different from those in the Late Triassic–Late Jurassic, and the OtogQianqi–GT1 wellblocks could be divided into two units. Further hydrocarbon generation within the double rifts and oil–gas reservoir readjustment led to oil–gas accumulation in the unconformity-related traps within the Beidajian Fm. In the OtogQianqi region. During the readjustment period since the Late Cretaceous, the OtogQianqi unit and its adjacent units to the northeast became integrated. The early-formed hydrocarbon reservoirs in the eastern part of OtogQianqi shifted towards the northeast unconformity-related traps on a large scale, while the oil–gas reservoirs in the northern part of OtogQianqi shifted towards the northern region by a short distance.

Using the above-mentioned analysis method, the type of hydrocarbon accumulation in each period was determined, such as multi-stage accumulation, accumulation leakage and residue, and accumulation readjustment or replenishment. The simulation results of the hydrocarbon accumulation during each period were superimposed in a single stratum according to the chronological order and spatial position. Finally, considering the reserves and types of each oil–gas accumulation, the favorable areas were systematically identified.

The superimposed map of the hydrocarbon accumulation within the Changcheng System indicates that the current hydrocarbon accumulation zone to the south of well E6 can potentially reach 70.8 MMbbls. This accumulation zone is located in the unconformity-related traps within the Beidajian Fm. and is the result of multiple periods of accumulation in T–J and accumulation readjustment in K_2–Q (Fig. 21(a); Table 5). The current oil–gas accumulation, located within the unconformity-related traps in the Beidajian Fm. In the area to the north of well T59 and the area to the south of well T93, is characterized by leakage and residue in the Jurassic strata, followed by readjustment and replenishment in K_2–Q. These accumulation zones contain reserves of 2.7 and 8.6 MMbbls, respectively. The current hydrocarbon accumulation in the JGT1 wellblock is the result of readjustment of the K_1 hydrocarbon accumulation in the northern part of Dingbian during K_2–Q, and its reserves are relatively small, amounting to only 0.4 MMbbls. Integration of the regional geologic setting and some petroleum geology data suggests that the structural highs and unconformity-controlled traps in the Changcheng System are of crucial importance for current oil exploration.

The superimposed map of the hydrocarbon accumulation within the Cambrian strata suggests that there were multiple periods of inherited accumulation in the L73–L1–XT1 wellblocks, which contain significant reserves. The largest accumulation zone, containing reserves of up to 893.4 MMbbls, is located in the area to the north of well L1 (Fig. 21(b); Table 5). These zones may be pivotal areas for current oil exploration. However, it should be noted that thrust faults have developed in these areas, and the accuracy of the 3-D basin modeling with thrust faults is poor, and thus the accuracy of the locations of the oil–gas accumulations in these areas needs to be confirmed through 2-D simulation. The Cambrian weathering crust in the Huanxian–Yan'an area contains

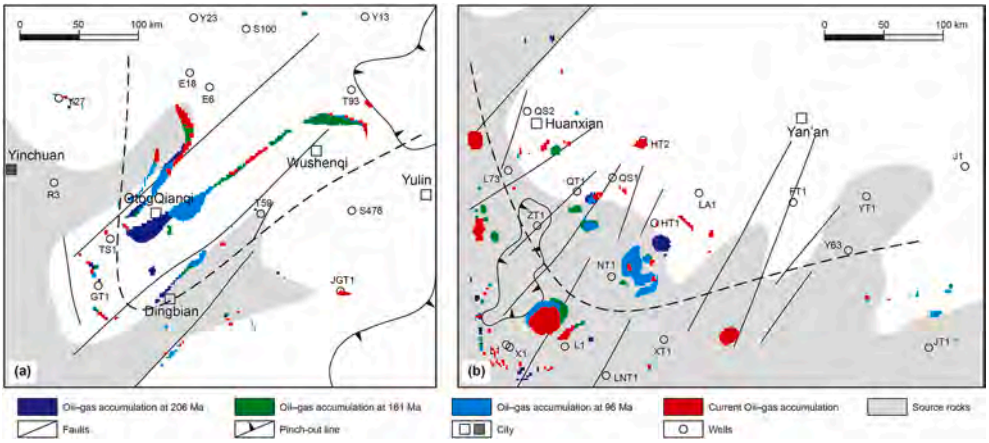

Fig. 21. Superimposed map of inherited oil–gas accumulaltions of different periods in the **(a)** Changcheng System and **(b)** Cambrian for the Mesoproterozoic petroleum system.

Table 5
Reserves and type description based on the simulation of the Mesoproterozoic petroleum system in the Ordos Basin.

Hydrocarbon accumulation area		Reservoir	Play	Reserves, MMbbls	Type description
Ding–Wu system	South of Well T93	Beidajian Fm.	Beidajian stratigraphic–structural	8.6	Early leakage and residue, late readjustment and replenishment
	North of Well T59	Beidajian Fm.	Beidajian stratigraphic–structural	2.7	Early leakage and residue, late readjustment and replenishment
	South of Well E6	Beidajian Fm.	Beidajian stratigraphic–structural	70.8	Multi-period accumulation
	Well JGT1	Beidajian Fm.	Beidajian stratigraphic–structural	0.4	Late natural gas readjustment
Huan–Yan system	QS2–NT1–LA1 Wellblocks	Sanhsanzi–Zhangxia Fms.	Cambrian carbonate stratigraphic–structural	302.1	Late natural gas readjustment
	North of Well L73	Sanshanzi Fm.	Sanshanzi clastic structural	302.1	Multi-period accumulation
	South of Well L73	Zhangxia Fm.	Zhangxia clastic structural	232.4	Multi-period accumulation
	North of Well L1	Zhangxia Fm.	Zhangxia carbonate structural	893.4	Multi-period accumulation
	East of Well XT1	Sanshanzi Fm.	Sanshanzi clastic structural	423.2	Multi-period accumulation

significant oil–gas accumulation, with reserves of up to 302.1 MMbbls. These accumulation zones are attributed to the readjustment of the hydrocarbon accumulation in the T–K_1 during K_2–Q. In recent years, numerous hydrocarbon shows and low production gas reservoirs have been drilled in the top of the Cambrian weathering crust in this region (Du et al., 2019; Li et al., 2021; Wu et al., 2024b). While the Cambrian–Ordovician and Upper Paleozoic source rocks do impact the oil–gas accumulation in this region, it is important to acknowledge the significant contribution of the Mesoproterozoic petroleum system.

5.6. Proposed approach for Mesoproterozoic petroleum system

The traditional "four figures and one table" approach for petroleum systems consists of a burial history map, plan view of the critical period, profile of the critical period, accumulation events chart, and reserves and type description table. However, these components are inadequate for investigating Mesoproterozoic petroleum system characterized by multistage hydrocarbon accumulation. Based on the nested simulation of local grid refinement and in conjunction with a systematic analysis of the hydrocarbon accumulation process conducted unit by unit and period by period, we propose a "five figures and one table" approach for characterizing complex Mesoproterozoic petroleum system, including a burial history map, accumulation events chart, plan view of multi-critical periods, profile of multi-critical periods, superimposed map of hydrocarbon accumulation during different periods in a single stratum, and reserves and type description table of discoveries or simulations.

Nested simulation of local grid refinement can establish a connection between widely-distributed source rocks and the target area. If the geological model of the target area is relatively detailed, accurate specification of hydrocarbon injection timings, fluxes, modes, and positions along the outer boundary of the target area is required. This can be achieved by adding additional grids into the parent model and introducing additional coupling conditions. In this simulation, given the relatively limited number of hydrocarbon sources outside the target area, applying this method for nested simulation resulted in a significant change in oil–gas accumulation within the Cambrian weathering crust of the Huanxian–Yan'an area (QS2–NT1–LA1 wellblocks), increasing from 287.2 MMbbls before the addition of additional grids and introduction of additional coupling conditions to 302.1 MMbbls afterward. This is primarily due to the fact that this approach enables a more accurate and efficient injection of hydrocarbons generated outside the child model into the target area. It is evident that if there are numerous hydrocarbon sources outside the target area, this may lead to significantly different simulation results.

In this study, the evolution of Mesoproterozoic petroleum system, characterized by multiple stages of hydrocarbon accumulation, was reconstructed based on the hydrocarbon migration simulation at the scale of the hydrocarbon migration and accumulation system, which was nested within the evolution simulation of the source rocks at the scale of the petroleum system. This

was achieved using profiles and plan views of the multiple critical periods so as to analyze the spatiotemporal variations in the geologic factors and processes. Focusing on these multiple critical periods of hydrocarbon accumulation, we analyzed the influences of various factors on the simulation results for each period based on the concept of migration and accumulation units. The simulation results for the hydrocarbon accumulation during each period were superimposed in a single stratum according to their chronological order and spatial position. This approach enabled us to determine the type and characteristics of each hydrocarbon accumulation pool in each period, thereby allowing us to establish a reserves and type description table based on the discovered and simulated oil–gas reservoirs. This description table and the superimposed map served as the core of the Mesoproterozoic petroleum system evaluation, providing valuable insights for systematically identifying potential favorable areas.

Nested simulation and the concept of migration and accumulation units represent an effective method for analyzing Meso–Neoproterozoic petroleum systems. The use of the “five figures and one table” approach allows for attainment of a dynamic description of the evolution process of the Meso–Neoproterozoic petroleum systems, as well as a systematic evaluation of the advantages and disadvantages of potential favorable areas. This is a novel method for analyzing Meso–Neoproterozoic petroleum systems.

6. Conclusions

In this study, the following findings were obtained.

(1) Nested simulation, which involves adding additional grids into the parent model and introducing additional coupling conditions, ensures accurate representation of the temporal and spatial distribution and quantity of hydrocarbon supply, enhances the resolution of lithological and structural details in the target area, and supports the evaluation of potential favorable exploration areas. The use of a “five figures and one table” approach can effectively illustrate the complex Meso–Neoproterozoic petroleum systems, and is a novel approach for analyzing a petroleum system characterized by multistage hydrocarbon accumulation.

(2) The source rocks in the Changcheng System have significant hydrocarbon generation potential, and high-quality source rocks have been formed in the deep rift region as a result of submarine hydrothermal activity and the presence of anoxic bottom waters. The reservoir rocks in the Changcheng System typically consist of tight sandstone. Owing to the high structural and compositional maturity (littoral–neritic facies), combined with the presence of pore-lining clay or feldspar dissolution, favorable reservoir rocks have been developed, particularly in the Baicaoping Formation in the central basin.

(3) The plan views and profiles for multiple critical periods indicate that the location of the Central Paleohigh controlled the hydrocarbon migration and accumulation in the petroleum system during the Triassic–Early Cretaceous. During this time, the hydrocarbon reservoirs were primarily distributed within the paleohigh and its adjacent regions. Oil and gas readjustment and re-accumulation have occurred along the unconformities toward the northeast region on a large scale since the Late Cretaceous, and these processes were the most significant in the Dingbian–Yulin area.

(4) Integration of the regional geologic setting and available petroleum geology data suggests that in the Changcheng System, the structural highs and unconformity-related traps are of crucial importance for current oil exploration. The Cambrian weathering crust in the Huanxian–Yan'an area contains abundant oil–gas shows, and it is important to acknowledge the significant contribution of the Mesoproterozoic petroleum system. The results of this study provide essential insights for future hydrocarbon exploration in the Ordos Basin.

CRediT authorship contribution statement

Kuai-Le Zhang: Writing – original draft, Methodology, Formal analysis, Conceptualization. **Zhen-Liang Wang:** Writing – review & editing, Investigation. **Xiao-Rong Luo:** Supervision, Funding acquisition. **Xing Pan:** Resources. **Li-Yong Fan:** Resources, Project administration. **Zhan-Rong Ma:** Resources.

Declaration of interest statement

The authors declare that they have no known competing financial interests or personal relationships that could have appeared to influence the work reported in this paper.

Acknowledgements

We acknowledge the generous funding from the National Natural Science Foundation of China (Grant No. 42302151 and Grant No. 42572180) and the PetroChina Changqing Oilfield Innovation Consortium Project (Grant No. 2024D1JC06). We also thank Editor Xiufang Hu and seven anonymous reviewers for their constructive comments and suggestions that greatly improve the quality of the manuscript.

References

Bai, H.F., Bao, H.P., Li, Z.M., Hao, S.L., Wu, C.Y., Jing, X.H., 2020. Sedimentary characteristics and gas accumulation potential of Changcheng system in the Ordos Basin in Proterozoic. Chin. J. Geol. 55 (3), 672–691. https://doi.org/10.12017/dzkx.2020.041 (in Chinese).

Bai, J.L., Zhao, J.F., Ren, Z.L., Li, W.H., Wang, K., Li, X., 2022. Paleogeographic and sedimentary evolution of Meso–Neoproterozoic strata in the Ordos Basin, Western North China Craton. J. Petrol. Sci. Eng. 215, 110600. https://doi.org/10.1016/j.petrol.2022.110600.

Bora, D., Dubey, S., 2015. New insight on petroleum system modeling of Ghadames Basin, Libya. J. Afr. Earth Sci. 112, 111–128. https://doi.org/10.1016/j.jafrearsci.2015.08.020.

Butterfield, N.J., 2015. Early evolution of the eukaryota. Palaeontology 58 (1), 5–17. https://doi.org/10.1111/pala.12139.

Chen, J.F., Sun, S.L., Liu, W.H., Zhang, J.J., 2004. Geochemical characteristics of organic matter-rich strata of lower Cambrian in Tarim Basin and its origin. Sci. China Ser. D Earth Sci. 47 (S2), 125–132. https://doi.org/10.1360/04zd0031.

Chen, Q.H., 2007. Research on Sedimentary Systems and Hydrocarbons Enrichment of the Upper Paleozoic of the Ordos Basin. Ph.D. thesis. Northwestern University, Shaanxi, China (in Chinese).

Chen, R.Y., Luo, X.R., Chen, Z.K., Yu, J., Yang, Y., 2006. Restoration of burial history of four periods in Ordos Basin. Acta Pet. Sin. 27 (2), 43–47 (in Chinese).

Chen, Y.Z., 2015. The Tectonic Evolution Characteristics of Southern Margin of Ordos Block in Mesoproterozoic. Ph.D. Thesis. Zhejiang University, Zhejiang, China (in Chinese).

Chen, Z.X., Zhang, F.Q., Zhao, Z.Y., Gao, J.R., Li, C.S., Fu, L., Zhang, L.X., 2023. Characteristics of Lower Paleozoic Ordovician inclusions and oil and gas filling history in the Western margin of Ordos Basin. Nat. Gas Geosci. 34 (6), 1028–1038. https://doi.org/10.11764/j.issn.1672-1926.2023.01.005 (in Chinese).

Cox, G.M., Jarrett, A., Edwards, D., Edwards, D., Crockford, P.W., Collins, A.S., Poirier, A., Li, Z.X., 2016. Basin redox and primary productivity within the Mesoproterozoic roper seaway. Chem. Geol. 440, 101–114. https://doi.org/10.1016/j.chemgeo.2016.06.025.

Craig, J., Biffi, U., Galimberti, R.F., Ghori, K.A.R., Gorter, J.D., Hakhoo, N., Heron, D.P.L., Thurow, J., 2013. The palaeobiology and geochemistry of Precambrian hydrocarbon source rocks. Mar. Petrol. Geol. 40, 1–47. https://doi.org/10.1016/j.marpetgeo.2012.09.011.

Craig, J., Thurow, J., Thusu, B., Whitham, A., Abutarruma, Y., 2009. Global Neoproterozoic petroleum systems: The emerging potential in North Africa. Geol. Soc., Lond., Spec. Publ. 326 (1), 1–25. https://doi.org/10.1144/SP326.

Cui, M.L., Zhang, B.L., Zhang, L.C., 2011. U–Pb dating of baddeleyite and zircon from the Shizhaogou diorite in the southern margin of the North China Craton: Constraints on the timing and tectonic setting of the Paleoproterozoic Xiong'er group. Gondwana. Res. 20, 184–193. https://doi.org/10.1016/j.gr.2011.01.010.

Dean, W.E., Gardner, J.V., Piper, D.Z., 1997. Inorganic geochemical indicators of glacial–interglacial changes in productivity and anoxia on the California continental margin. Geochem. Cosmochim. Acta 61 (21), 4507–4518. https://doi.org/10.1016/S0016-7037(97)00237-8.

Diwu, C.R., Sun, Y., Yuan, H.L., Wang, H.L., Zhong, X.P., Liu, X.M., 2008. U–Pb ages and Hf isotopes for detrital zircons from quartzite in the Paleoproterozoic Songshan Group on the southwestern margin of the North China Craton. Chin. Sci. Bull. 53, 2828–2839. https://doi.org/10.1007/s11434-008-0342-1.

Dow, W.G., 1974. Application of oil-correlation and source-rock data to exploration in Williston Basin. AAPG Bull. 58 (7), 1253–1262. https://doi.org/10.1306/83D91655-16C7-11D7-8645000102C1865D.

Du, J.H., Li, X.B., Bao, H.P., Xu, W.L., Wang, Y.T., Huang, J.P., Wang, H.B., Wan-Yan, R., Wang, J., 2019. Geological conditions of natural gas accumulation and new exploration areas in the Mesoproterozoic to lower Paleozoic of Ordos Basin, NW China. Petrol. Explor. Dev. 46 (5), 866–882. https://doi.org/10.1016/S1876-3804(19)60246-6.

Duran, E.R., di Primio, R., Anka, Z., Stoddart, D., Horsfield, B., 2013. 3D-basin modelling of the Hammerfest Basin (southwestern Barents Sea): A quantitative assessment of petroleum generation, migration and leakage. Mar. Petrol. Geol. 45, 281–303. https://doi.org/10.1016/j.marpetgeo.2013.04.023.

Faiz, M., Altmann, C., Baruch, E., Côté, A., Gong, S., Schinteie, R., Ranasinghe, P., 2022. Organic matter composition and thermal maturity evaluation of Mesoproterozoic source rocks in the Beetaloo Sub-Basin, Australia. Org. Geochem. 174, 104513. https://doi.org/10.1016/j.orggeochem.2022.104513.

Fan, L.Y., Shi, Y.H., Dong, G.D., Zhang, J.Y., Pan, B., Wang, Y.Q., 2024. Geochemical characteristics and coal-forming environments of deep coal rocks of Permian Shanxi Formation in central and eastern Ordos Basin. Nat. Gas. Ind. 44 (10), 113–125. https://doi.org/10.3787/j.issn.1000-0976.2024.10.009 (in Chinese).

Feng, J.P., Ding, X.F., Ouyang, Z.J., 2015. Geochemical characteristics of Mesoproterozoic Erathem Changchengian system source rocks in the south margins of Ordos Basin. J. Xi'an Univ. Sci. Technol. 35 (6), 749–754. https://doi.org/10.13800/j.cnk.xakjdxxb.2015.0613 (in Chinese).

Feng, J.P., Ouyang, Z.J., Fan, M.M., 2020. Geological characteristics and significance of source rocks of Mesoproterozoic Changchengian system in north of Guyang County of the northern margin of Ordos Basin. Chin. J. Geol. 55 (4), 1044–1055. https://doi.org/10.12017/dzkx.2020.064 (in Chinese).

Feng, J.P., Yao, W.Z., Ouyang, Z.J., Li, W.H., 2024. Geological characteristics of source rocks of Mesoproterozoic Changchengian system in Shujigou area of the northern margin of Ordos Basin. J. NW Univ. 54 (6), 950–960. https://doi.org/10.16152/j.cnki.xdxbzr.2024-06-002 (in Chinese).

Frolov, S.V., Akhmanov, G.G., Bakay, E.A., Lubnina, N.V., Korobova, N.I., Karnyushina, E.E., Kozlova, E.V., 2015. Meso–Neoproterozoic petroleum systems of the eastern Siberian sedimentary basins. Precambr. Res. 259, 95–113. https://doi.org/10.1016/j.precamres.2014.11.018.

Fu, J.H., Fan, L.Y., Liu, X.S., Hu, X.Y., Li, J.H., Ji, H.K., 2019. New progresses, prospects and countermeasures of natural gas exploration in the Ordos Basin. China Petrol. Explor 24 (4), 418–430. https://doi.org/10.3969/j.issn.1672-7703.2019.04.002 (in Chinese).

Fu, J.H., Li, S.X., Liu, X.Y., 2013. Geological theory and practice of petroleum exploration in the Ordos Basin. Nat. Gas Geosci. 24 (6), 1091–1101. https://doi.org/10.11764/j.issn.1672-1926.2013.06.1091 (in Chinese).

Fu, J.H., Li, S.X., Xu, L.M., Niu, X.B., 2018. Paleo-sedimentary environmental restoration and its significance of Chang 7 Member of Triassic Yanchang Formation in Ordos Basin, NW China. Pertol. Exp. Dev. 45 (6), 998–1008. https://doi.org/10.1016/S1876-3804(18)30104-6.

Gao, J., Lv, D.W., Tom van Loon, A.J., Hower, J.C., Raji, M., Yang, Y., Ren, Z.H., Wang, Y.J., Zhang, Z.H., 2022. Reconstruction of provenance and tectonic setting of the Middle Jurrasic Yan'an Formation (Ordos Basin, North China) by analysis of major, trace and rare Earth elements in the coals. Ore Geol. Rev. 151, 105218. https://doi.org/10.1016/j.oregeorev.2022.105218.

Guo, Y.R., Fu, J.H., Wei, X.S., Xu, W.L., Sun, L.Y., Liu, J.B., Zhao, Z.Y., Zhang, Y.Q., Gao, J.R., Zhang, Y.L., 2014. Natural gas accumulation and models in Ordovician carbonates, Ordos Basin, NW China. Petrol. Explor. Dev. 41 (4), 437–448. https://doi.org/10.1016/S1876-3804(14)60050-1.

Guo, Y.R., Zhao, Z.Y., Zhang, Y.Q., Xu, W.L., Bao, H.P., Zhang, Y.L., Gao, J.R., Song, W., 2016. Development characteristics and new exploration areas of marine source rocks in Ordos Basin. Acta Pet. Sin. 37 (8), 939–951. https://doi.org/10.7623/syxb201608001 (in Chinese).

Hantschel, T., Kauerauf, A.I., 2009. Introduction to basin modeling. In: Fundamentals of Basin and Petroleum Systems Modelling. Springer-Verlag, Berlin/Heidelberg.

Hao, S.L., Sun, L.Y., Bao, H.P., Liu, G., Zhang, G.S., 2016. Exploration direction and potential of the Middle–Upper Proterozoic in Ordos Basin. Nat. Gas Geosci. 27 (12), 2127–2135. https://doi.org/10.11764/j.issn.1672-1926.2016.12.2127 (in Chinese).

Hatch, J.R., Leventhal, J.S., 1992. Relationship between inferred redox potential of the depositional environment and geochemistry of the upper Pennsylvanian (Missourian) Stark shale member of the Dennis Limestone, Wabaunsee County, Kansas, U.S.A. Chem. Geol. 99, 65–82. https://doi.org/10.1016/0009-2541(92)90031-Y.

Huang, J.P., Fan, L.Y., Zhang, Y., Ren, J.F., Shi, J.L., Jing, X.H., Wang, H.B., Li, X.B., Feng, M., Wang, J., 2025. Geological characteristics of natural gas accumulation in the Cambrian and exploration orientations in Ordos Basin. China Pet. Explor 30 (1), 98–110. https://doi.org/10.3969/j.issn.1672-7703.2025.01.008 (in Chinese).

Javaux, E.J., Knoll, A.H., Walter, M.R., 2001. Morphological and ecological complexity in early eukaryotic ecosystems. Nature 412 (6842), 66–69. https://doi.org/10.1038/35083562.

Jia, C.Z., Pang, X.Q., Song, Y., 2023. Whole petroleum system and ordered distribution pattern of conventional and unconventional oil and gas reservoirs. Pet. Sci. 20 (1), 1–19. https://doi.org/10.1016/j.petsci.2022.12.012.

Jiang, M., Shi, J.Y., Fan, T.L., Zhao, W.P., Wu, Z.C., Fan, J.H., 2023. Lithofacies and depositional settings of Mesoproterozoic shales: Insights from the ~1.65 Ga Chuanlinggou Formation, Yanliao Basin, North China Craton. Geoenergy Sci. Eng. 229, 211998. https://doi.org/10.1016/j.geoen.2023.211998.

Jin, Z.J., 2023. Hydrocarbon accumulation and resources evaluation: Recent advances and current challenges. Adv. Geo-Energy Res. 8 (1), 1–4. https://doi.org/10.46690/ager.2023.04.01.

Kai, B.Z., He, D.F., Ma, J.H., Xu, Y.H., Zhai, Y.H., Chang, X., 2020. Tectonic subsidence characteristics of Ordos Basin and its enlightenment to basin genesis. Chin. J. Geol. 55 (3), 657–671. https://doi.org/10.12017/dzkx.2020.040 (in Chinese).

Li, H.K., Su, W.B., Zhou, H.Y., Xiang, Z.Q., Tian, H., Yang, L.G., Huff, W.D., Ettensohn, F.R., 2014. The first precise age constraints on the Jixian System of the Meso–Neoproterozoic standard section of China: SHRIMP zircon U–Pb dating of bentonites from the Wumishan and Tieling formations in the Jixian section, North China Craton. Acta Petrol. Sin. 30 (10), 2999–3012 (in Chinese).

Li, M., Yan, X.B., Zhang, W., Guo, Y.L., Liu, C.Y., Fan, L.L., Yang, S., 2024. Characteristics and genetic mechanism of the Mesoproterozoic rift system, Ordos Basin, China. Energy Geosci 5 (1), 100221. https://doi.org/10.1016/j.engeos.2023.100221.

Li, R.X., Liang, J.W., Weng, K., 2011. Paleo-reservoir bitumen of the middle protozoic jixian system in the southwest margin of the ordos Basin, China. Petrol. Explor. Dev. 38 (2), 168–173. https://doi.org/10.1016/S1876-3804(11)60024-4.

Li, X.B., Wang, H.B., Huang, J.P., Zhang, C.L., Zhang, Y., Wang, Y.T., Zhang, L., Wang, J., Liu, H.Q., 2021. Characteristics of unconformity resulted from Huaiyuan Movement in Ordos Basin and its significance for oil and gas exploration. Oil Gas Geol. 42 (5), 1043–1055. https://doi.org/10.11743/ogg20210503 (in Chinese).

Li, Y.H., Li, W.H., Zhang, Q., 2020. Atlas of Sedimentary Facies of Ordos Basin and its Periphery. Geological Publishing House, Beijing (in Chinese).

Li, Z.H., Xi, S.L., Hu, J.M., Dong, X.P., Zhang, G.S., 2019. New insights about the Mesoproterozoic sedimentary framework of North China Craton. Geol. J. 54 (1), 409–425. https://doi.org/10.1002/gj.3190.

Liu, H.Y., Liu, M.J., Hao, Z.L., Ren, Y., Wu, E.Y., Xu, H., Zhong, S.K., Tan, X.C., Zeng, W., Lian, C.B., Dai, H.M., 2024. Pore formation and preservation mechanisms of ancient deep tight sandstone reservoirs:a case study of the Mesoproterozoic Changcheng system in Ordos Basin. J. Palaeogeogr. (Chin. Ed.) 6, 1435–1451. https://doi.org/10.7605/gdlxb.2024.05.088 (in Chinese).

Liu, Y., Zhong, N.N., Tian, Y.J., Qi, W., Mu, G.Y., 2011. The oldest oil accumulation in China: Meso-proterozoic Xiamaling Formation bituminous sandstone reservoirs. Petrol. Explor. Dev. 38 (4), 503–512. https://doi.org/10.1016/S1876-3804(11)60050-5.

Lu, S.N., Zhao, G.C., Wang, H.C., Hao, G.J., 2008. Precambrian metamorphic basement and sedimentary cover of the North China Craton: A review. Precambr. Res. 160, 77–93. https://doi.org/10.1016/j.precamres.2007.04.017.

Luo, Q.Y., George, S.C., Xu, Y.H., Zhong, N.N., 2016. Organic geochemical characteristics of the Mesoproterozoic Hongshuizhuang Formation from northern China: Implications for thermal maturity and biological sources. Org. Geochem. 99, 23–37. https://doi.org/10.1016/j.orggeochem.2016.05.004.

Luo, X.R., 2008. Understandings on dynamical studies of hydrocarbon migration and accumulation. Nat. Gas Geosci. 19, 149–156. https://doi.org/10.11764/j.issn.1672-1926.2008.02.149 (in Chinese).

Luo, X.R., Zhang, L.K., Lei, Y.H., Yang, W., 2020. Petroleum migration and accumulation: Modeling and applications. AAPG Bull. 104 (11), 2247–2265. https://doi.org/10.1306/0422201618817104.

Magenheim, A.J., Gieskes, J.M., 1992. Hydrothermal discharge and alteration in near surface sediments from the Guaymas Basin, Gulf of California. Geochem. Cosmochim. Acta 56, 2329–2338. https://doi.org/10.1016/0016-7037(92)90192-L.

Magoon, L.B., Dow, W.G., 1994. The Petroleum System: From Source to Trap. American Association of Petroleum Geologists, Tulsa.

Magoon, L.B., Schmoker, J.W., 2000. The Total Petroleum System: The Natural Fluid Network that Constrains the Assessment Unit: USGS World Energy Assessment Team. U.S. Geological Survey Digital Data Series 60. U.S. Geological Survey, Reston, VA.

McKenzie, D., 1978. Some remarks on the development of sedimentary basins. Earth Planet Sci. Lett. 40 (1), 25–32. https://doi.org/10.1016/0012-821X(78)90071-7.

McManus, J., Berelson, W.M., Klinkhammer, G.P., Johnson, K.S., Coale, K.H., Anderson, R.F., Kumar, N., Burdige, D., Hammond, D., Brumsack, H.J., McCorkle, D., Rushdi, A.I., 1999. Geochemistry of barium in marine sediments: Implications for its use as a paleoproxy. Geochem. Cosmochim. Acta 62 (21–22), 3453–3473. https://doi.org/10.1016/S0016-7037(98)00248-8.

Meng, F.W., Zhou, C.M., Yan, X., Yuan, X.L., Yin, L.M., 2006. Biological origin of early Palaeozoic and Precambrian hydrocarbon source rocks based on C27/C29 sterane ratio and organic carbon isotope. Acta Micropalaeontol. Sin. 23 (1), 51–56 (in Chinese).

Pan, X., Wang, Z.L., Li, Q.Y., Gao, J., Zhu, L.W., Liu, W.H., 2020. Sedimentary environments and mechanism of organic matter enrichment of dark shales with low TOC in the Mesoproterozoic Cuizhuang Formation of the Ordos Basin: Evidence from petrology, organic geochemistry, and major and trace elements. Mar. Petrol. Geol. 122, 104695. https://doi.org/10.1016/j.marpetgeo.2020.104695.

Peng, P., Zhai, M.G., Li, Q.L., Wu, F.Y., Hou, Q.L., Li, Z., Li, T.S., 2011. Neoproterozoic (~900Ma) sariwon sills in North Korea: Geochronology, geochemistry and

implications for the evolutions of the southeastern margin of the North China Craton. Gondwana Res. 20, 243–354. https://doi.org/10.1016/j.gr.2010.12.011.
Peng, Z.M., Wu, Z.P., 2006. Development features of Triassic strata and analysis of original sedmientary pattern in North China. Geol. J. China Univ. 12 (3), 343–352. https://doi.org/10.16108/j.issn1006-7493.2006.03.006 (in Chinese).
Pepper, A.S., Corvi, P.J., 1995. Simple kinetic models of petroleum formation. Part I: Oil and gas generation from kerogen. Mar. Petrol. Geol. 12 (3), 291–319. https://doi.org/10.1016/0264-8172(95)98381-E.
Pollastro, R.M., Jarvie, D.M., Hill, R.J., Adams, C.W., 2007. Geologic framework of the Mississippian Barnett shale, Barnett–Paleozoic total petroleum system, Bend arch–Fort Worth Basin, Texas. AAPG Bull. 91 (4), 405–436. https://doi.org/10.1306/10300606008.
Qi, K., 2018. A Preliminary Study of Meso-Cenozoic Thermal Regime and Lithospheric Dynamic Evolution in the Ordos Basin, WNCC. MPhil Diss, Northwestern University, Shaanxi, China (in Chinese).
Qi, K., Ren, Z.L., Cui, J.P., Yu, Q., 2020. Meso-Cenozoic lithospheric thermal structure and its significance in the evolution of the lithosphere in the Ordos Basin, WNCC, China. Int. Geol. Rev. 63 (3), 1–20. https://doi.org/10.1080/00206814.2020.1827459.
Qin, J.Z., Zhen, L.J., Teng, G.E., 2007. Study on the restitution coefficient of original total organic carbon for high mature marine hydrocarbon source rocks. Front. Earth Sci. China 1 (4), 482–490. https://doi.org/10.1007/s11707-007-0059-5.
Qu, H.J., Li, P., Dong, Y.P., Yang, B., Chen, S., Han, X., Wang, K., He, M., 2020. Development and distribution rules of the main Neoproterozoic source and reservoir strata in the Yangtze Block, Southern China. Precambr. Res. 350, 105915. https://doi.org/10.1016/j.precamres.2020.105915.
Ren, Z.l., Qi, K., Liu, R.C., Cui, J.P., Zhang, Y.Y., Yang, G.L., Ma, Q., 2020. Dynamic background of Early Cretaceous tectonic thermal events and its control on various mineral accumulations such as oil and gas in the Ordos Basin. Acta Pet. Sin. 36 (4), 1213–1234. https://doi.org/10.18654/1000-0569/2020.04.15 (in Chinese).
Rimmer, S.M., 2004. Geochemical paleoredox indicators in Devonian–Mississippian black shales, central Appalachian Basin (USA). Chem. Geol. 206 (3–4), 373–391. https://doi.org/10.1016/j.chemgeo.2003.12.029.
Santos, R.V., de Alvarenga, C.J.S., Dardenne, M.A., Sial, A.N., Ferreira, V.P., 2000. Carbon and oxygen isotope profiles across Meso-neoproterozoic limestones from central Brazil: Bambui and Paranoa groups. Precambr. Res. 104 (3–4), 107–122. https://doi.org/10.1016/S0301-9268(00)00082-6.
Schmitz, B., 1987. Barium, equatorial high productivity and the northward wandering of the Indian continent. Paleoceanography 2 (1), 63–77. https://doi.org/10.1029/PA002i001p00063.
Tang, D.J., Shi, X.Y., Wang, X.Q., Jiang, G.Q., 2016. Extremely low oxygen concentration in mid-proterozoic shallow seawaters. Precambr. Res. 276, 145–157. https://doi.org/10.1016/j.precamres.2016.02.005.
Wang, G.Z., Li, S.Z., Li, X.Y., Zhao, W.Z., Zhao, S.J., Suo, Y.H., Liu, X.G., Somerville, I., Liu, Y.M., Zhou, J., Wang, Z.C., 2019. Destruction effect on Meso–Neoproterozoic oil-gas traps derived from Meso–Cenozoic deformation in the North China Craton. Precambr. Res. 333, 105427. https://doi.org/10.1016/j.precamres.2019.105427.
Wang, J., Chen, J.F., Bao, Z.D., Zhang, S.C., Xu, Y.C., 2006. Influences of marine floor hydrothermal activity on organic matter abundance in marine carbonate rocks — a case study of middle–upper Proterozoic in the northern part of North China. Chin. Sci. Bull. 51 (5), 585–593. https://doi.org/10.1007/s11434-006-0585-7.
Wang, K., Wang, T.S., Wang, Z.C., Luo, P., Li, Q.F., Fang, J., Ma, K., 2018. Characteristics of the Changchengian rifts in the southern margin of North China Craton and its hydrocarbon geological conditions. Pet. Res. 3 (3), 269–282. https://doi.org/10.1016/j.ptlrs.2018.05.002.
Wang, T.G., Han, K.Y., 2011. On Meso-Neoproterozoic primary petroleum resources. Acta Pet. Sin. 32 (1), 1–7 (in Chinese).
Wang, T.G., Zhong, N.N., Wang, C.J., Zhu, Y.X., Liu, Y., Song, D., 2022. Source beds and oil charging to alteration histories of fossil-oil-reservoirs in the basal sandstone of Xiamaling Formation, Jibei Depression. In: Meso-Neoproterozoic Geology and Petroleum Resources in China. Springer Geology. Springer, Singapore, pp. 461–484. https://doi.org/10.1007/978-981-19-5666-9_12.
Wang, X.M., Zhang, S.C., Wang, J.H., Su, J., He, K., Wang, Y., Wang, X.Q., 2017. Significance of source rock heterogeneities: A case study of Mesoproterozoic Xiamaling Formation shale in North China. Pertol. Exp. Dev. 44 (1), 32–39. https://doi.org/10.1016/S1876-3804(17)30005-8.
Wang, X.M., Zhang, S.C., Ye, Y.T., Ma, S.H., Su, J., Wang, H.J., Canfield, D.E., 2023. Nitrogen cycling during the Mesoproterozoic as informed by the 1400 million year old Xiamaling Formation. Earth Sci. Rev. 243, 104499. https://doi.org/10.1016/j.earscirev.2023.104499.
Wang, Y.P., Chen, L.Q., Yang, G.Y., Wu, L., Xiao, A.C., Zhou, Y.J., Sun, L.Y., Zhang, C.L., Yang, S.F., Chen, H.L., 2021. The late Paleoproterozoic to Mesoproterozoic rift system in the Ordos Basin and its tectonic implications: Insight from analyses of bouguer gravity anomalies. Precambr. Res. 352, 105964. https://doi.org/10.1016/j.precamres.2020.105964.
Wu, C., Liu, B., Wei, L.B., Lu, F.F., Shi, K.B., 2024b. The restoration of palaeokarst geomorphology during Huaiyuan movement and its petroleum geological significance in Ordos basin. Chin. J. Geol. 59 (3), 732–743. https://doi.org/10.12017/dzkx.2024.052 (in Chinese).
Wu, Z.C., Shi, J.Y., Fan, T.L., Jiang, M., 2024a. Sedimentary paleoenvironment and its control on organic matter enrichment in the Mesoproterozoic hydrocarbon source rocks in the Ordos basin, southern margin of the North China Craton. Pet. Sci. 21 (4), 2257–2272. https://doi.org/10.1016/j.petsci.2024.03.009.
Wygrala, B.P., 1989. Integrated Study of an Oil Field in the Southern Po Basin, Northern Italy. Berichte des Forschungszentrums Juelich, Juelich, Germany. Ph.D. thesis.
Xu, Y., Sepehrnoori, K., 2022. Modeling fracture transient flow using the embedded discrete Fracture model with nested local grid refinement. J. Petrol. Sci. Eng. 218, 110882. https://doi.org/10.1016/j.petrol.2022.110882.
Xu, Y.H., He, D.F., 2022. Triassic provenance shifts and tectonic evolution of southeast Ordos basin, central China. Palaeogeogr. Palaeoclimatol. Palaeoecol. 598, 111002. https://doi.org/10.1016/j.palaeo.2022.111002.
Yang, H., Fu, J.H., Chen, H.D., 2012b. Sedimentary Geology and Hydrocarbons Distribution in the Late Triassic, Ordos Basin. Science Press, Beijing (in Chinese).
Yang, H., Fu, J.H., Liu, X.S., Fan, L.Y., 2012a. Formation conditions and exploration technology of large-scale tight sandstone gas reservoir in Sulige. Acta Pet. Sin. 33 (Suppl. 1), 27–36 (in Chinese).
Yang, H., Liu, X.S., 2014. Progress of Paleozoic coal-derived gas exploration in Ordos Basin, West China. Petrol. Explor. Dev. 41 (2), 129–137. https://doi.org/10.1016/S1876-3804(14)60017-3.
Yang, P., Ren, Z.L., Fu, J.H., Bao, H.P., Xiao, H., Shi, Z., Wang, K., Zhang, Y.Y., Liu, W.H., Li, W.H., 2024a. A tectono-thermal perspective on the petroleum generation, accumulation and preservation in the southern ordos basin, North China. Pet. Sci. 21 (3), 1459–1473. https://doi.org/10.1016/j.petsci.2023.12.006.
Yang, P., Ren, Z.L., Nuriel, P., Nguyen, A.D., Feng, Y.X., Zhou, R.J., Zhao, J.X., 2024b. Cenozoic faulting leading to petroleum escape in SW Ordos Basin, China: evidence from fault-related calcite in situ U–Pb dating, rare Earth elements and fluid inclusions. Mar. Petrol. Geol. 170, 107071. https://doi.org/10.1016/j.marpetgeo.2024.107071.
Yang, P., Ren, Z.L., Zhao, J.X., Nguyen, A.D., Feng, Y.X., Qi, K., Wang, K., 2021b. Tectonic evolution analysis constrained jointly by in-situ calcite U–Pb dating and apatite fission track for Southwestern Ordos Basin. Oil Gas Geol. 42 (5), 1189–1201. https://doi.org/10.11743/ogg20210516 (in Chinese).
Yang, P., Ren, Z.L., Zhou, R.J., Cui, J.P., Qi, L., Fu, J.H., Li, J.B., Liu, X.S., Li, W.H., Wang, K., 2021a. Tectonic evolution and controls on natural gas generation and accumulation in the Ordovician system of the Ordos Basin, North China. Energy Rep. 7, 6887–6898. https://doi.org/10.1016/j.egyr.2021.10.066.
Yuan, Y.S., Hao, Y.Q., Zhang, R.Q., 2024. Dynamic evaluation on sealing capacity of caprocks of the Meso-neoproterozoic reservoirs in Ordos Basin, China. Energy Geosci 5 (1), 100226. https://doi.org/10.1016/j.engeos.2023.100226.
Zhai, M.G., 2010. Tectonic evolution and metallogenesis of north China craton. Miner. Depos. 29 (1), 24–36.
Zhai, M.G., Hu, B., Peng, P., Zhao, T.P., 2014. Meso–neoproterozoic magmatic events and multi-stage rifting in the NCC. Earth Sci. Front. 21, 100–119 (in Chinese).
Zhang, S.H., Zhao, Y., Santosh, M., 2012. Mid-mesoproterozoic bimodal magmatic rocks in the northern North China Craton: Implications for magmatism related to breakup of the Columbia supercontinent. Precambr. Res. 222–223, 339–367. https://doi.org/10.1016/j.precamres.2011.06.003.
Zhang, S.H., Zhao, Y., Ye, H., Hu, J.M., Wu, F., 2013. New constraints on ages of the chuanlinggou and Tuanshanzi Formations of the Changcheng system in the Yan-Liao area in the northern North China Craton. Acta Pet. Sin. 29 (7), 2481–2490 (in Chinese).
Zhang, W., Pan, Y., Wang, J.S., Santo, V.D., Lauder, G.V., Dong, H.B., 2023. An efficient tree-topological local mesh refinement on Cartesian grids for multiple moving objects in incompressible flow. J. Comput. Phys. 479, 111983. https://doi.org/10.1016/j.jcp.2023.111983.
Zhao, G.C., He, Y.H., Sun, M., 2009. The Xiong'er volcanic belt at the southern margin of the North China Craton: Petrographic and geochemical evidence for its outboard position in the Paleo-Mesoproterozoic Columbia supercontinent. Gondwana Res. 16, 170–181. https://doi.org/10.1016/j.gr.2009.02.004.
Zhao, G.C., Sun, M., Wilde, S.A., 2003. Major tectonic units of the North China Craton and their Paleoproterozoic assembly. Sci. China, Ser. A D. 46 (1), 23–38. https://doi.org/10.1360/03yd9003.
Zhao, G.C., Wilde, S.A., Cawood, P.A., Sun, M., 2002. SHRIMP U–Pb zircon ages of the Fuping complex: Implications for late Archean to Paleoproterozoic accretion and assembly of the North China Craton. Am. J. Sci. 302, 191–226. https://doi.org/10.2475/ajs.302.3.191.
Zhao, W.Z., He, D.F., Chi, Y.L., Lei, Z.Y., Qu, H., 2001a. Major characteristics and exploration technology of multi-source petroleum systems in China. Acta Pet. Sin. 22 (1), 6–13 (in Chinese).
Zhao, W.Z., He, D.F., Qu, H., Lei, Z.Y., Chi, Y.L., 2001b. Study on the pathways of hydrocarbon migration of the composite petroleum system. Acta Pet. Sin. 22 (4), 7–12 (in Chinese).
Zhao, W.Z., Hu, S.Y., Wang, Z.C., Zhang, S.C., Wang, T.S., 2018. Petroleum geological conditions and exploration importance of Proterozoic to Cambrian in China. Petrol. Explor. Dev. 45 (1), 1–14. https://doi.org/10.1016/S1876-3804(18)30001-6.
Zhou, Y., Fu, S.Y., Zhang, T., Chen, H.D., Su, Z.T., Zhang, J.T., Zhang, C.G., Liu, Z.M., Han, X.Y., 2023. Tectono-sedimentary evolution, paleogeographic reconstruction and play fairway delineation of the Lower Paleozoic, Ordos Basin. Oil Gas Geol. 44 (2), 264–275. https://doi.org/10.11743/ogg20230202 (in Chinese).
Zhu, F.B., Zhou, H., 2018. Boimarker types and geochemical significance of crude oils in Western depression, Liaohe Basin. Earth Sci. 43 (2), 594–598. https://doi.org/10.3799/dqkx.2018.027 (in Chinese).
Zhu, G.Y., Zhang, Z.Y., Jiang, H., Chen, W.Y., Li, T.M., Li, X., 2024. Evolution of the Cryogenian cratonic basins in China, paleo-oceanic environment and hydrocarbon generation mechanism of ancient source rocks, and exploration potential in 10,000 m-deep strata. Earth Sci. Rev. 244, 104506. https://doi.org/10.1016/j.earscirev.2023.104506.